



Why does there occur spring predictability barrier for eastern Pacific El Niño but summer predictability barrier for central Pacific El Niño?

Can You^{1,2} · Meiyi Hou^{3,4} · Wansuo Duan^{1,2}

Received: 17 May 2024 / Accepted: 22 August 2024

© The Author(s), under exclusive licence to Springer-Verlag GmbH Germany, part of Springer Nature 2024

Abstract

Predictability barriers (PBs) significantly limit the prediction skill of the El Niño-Southern Oscillation (ENSO). The EP-El Niño predictions often encounter the impact of the spring PB, while the CP-El Niño predictions usually have PB phenomenon in summer. Using a data analysis approach for predictability dynamics and the pre-industrial control runs from the CCSM4 model outputs, the study explores the PB mechanism for EP- and CP-El Niño by tracing the evolution of initial errors. It is found that the significant spring PB for EP-El Niño and the notable summer PB for CP-El Niño often occur during the transition period from warm to cold phase of the initial sea surface temperature (SST) error evolution in the east-central tropical Pacific; however, there still exist respective initial errors that have specific spatial patterns leading to summer PB for EP-El Niño and spring PB for CP-El Niño. A comparison is made among the initial errors causing PBs for the two types of El Niño, and the results show that the initial errors resulting in the summer PB of CP-El Niño events tend to have more positive SST errors than those causing the spring PB for EP-El Niño in both the tropics and the Victoria mode (VM) region in the Northeast Pacific. These particular positive characteristics of the initial errors causing the summer PB pose a role that hinders the dissipation of the tropical Pacific positive SST errors and thus delay the spring transition phase of SST error, consequently triggering the occurrence of the summer PB for CP-El Niño. The role of the VM mode on SST in the tropical Pacific is inextricably linked to CP-El Niño formation and also sheds light on why the CP-El Niño tends to occur PB in summer. These findings provide a theoretical basis for advancing forecasting skills of El Niño diversity.

Keywords El Niño · Predictability barrier · Initial error · Prediction error

1 Introduction

The El Niño-Southern Oscillation (ENSO) phenomenon represents the most prominent interannual signal of ocean-atmosphere oscillation in the tropical Pacific Ocean, resulting from a combination of the El Niño phenomenon in the ocean and the Southern Oscillation phenomenon in the atmosphere (Bjerknes 1969; Rasmusson and Wallace 1983; Ropelewski and Halpert 1987). Its two phases, warm and cold, are known as El Niño and La Niña, respectively. Although ENSO occurs in the tropical Pacific, its global impact cannot be underestimated, as it can trigger extreme weather events, and even disasters, on a global scale (Chou and Lo 2007; Grimm and Tedeschi 2009; Zhang et al. 2011; Davey et al. 2014; Cao et al. 2017). Therefore, accurate prediction of ENSO is very important.

While significant progress has been made in understanding the dynamic mechanisms behind the ENSO phenomenon,

✉ Meiyi Hou
hmy@ynu.edu.cn

✉ Wansuo Duan
duanws@lasg.iap.ac.cn

¹ LASG, Institute of Atmospheric Physics, Chinese Academy of Sciences, Beijing 100029, China

² Collaborative Innovation Center on Forecast and Evaluation of Meteorological Disasters (CIC- FEMD), Nanjing University of Information Science and Technology, Nanjing 210044, China

³ Yunnan Key Laboratory of Meteorological Disasters and Climate Resources in the Greater Mekong Subregion, Yunnan University, Kunming 650500, China

⁴ Department of Atmospheric Sciences, Yunnan University, Kunming 650500, China

the real-time prediction skill of ENSO has not consistently improved (Neelin 1991; Levine and Jin 2010; Tang et al. 2018; Wang 2018; Ren et al. 2019). At the beginning of this century, the real-time prediction skill of ENSO was lower than in the 1980s and 1990s (Barnston et al. 2012; Tang et al. 2018). In a comparison of 30-year hindcasts between 1981 and 2010, the average correlation skill decreased from 0.65 to 0.42 with a lead time of 6 months (Barnston et al. 2012). Notably, the expected 2014 El Niño event did not occur, although most models predicted it would. In contrast, the 2015 El Niño, one of the strongest El Niño events on record, was not predicted by most models until a year before it occurred (McPhaden 2015). These examples illustrate the considerable uncertainty of real-time ENSO predictions.

The frequent occurrence of the new type of El Niño events since the 1990s poses new challenges for ENSO prediction (Masuda et al. 2015; Sohn et al. 2016). The traditional El Niño event is the eastern Pacific (EP-) El Niño, with its largest sea surface temperature (SST) anomaly in the EP. The new type of El Niño with its largest SST anomaly (SSTA) located near the dateline is known as central Pacific (CP-) El Niño (Yu and Kao 2007; Kao and Yu 2009; Kug et al. 2009). Previous studies have revealed that the CP-El Niño has different global climate impacts from the EP-El Niño (Zhang et al. 2011, 2012, 2016; Cai et al. 2020; Wang et al. 2021; Ge and Luo 2023). Therefore, it is necessary to distinguish the type of El Niño event in advance in the real-time predictions. However, many studies assessing the ability of prediction models to identify ENSO diversity obtained unsatisfactory results. Jeong et al. (2012) show that the APEC Climate Center's multi-model ensemble seasonal forecast system can distinguish between EP and CP-El Niño events within four months ahead. Lee et al. (2018) pointed out that many coupled general circulation models lose skills in predicting the El Niño type in advance for more than three months. Ren et al. (2019) emphasized that the EP- and CP-El Niño events can only be distinguished in some coupled models at a lead time of one month, even during boreal winter. Encouragingly, in a recent study, Zheng et al. (2023) embedded an ensemble nonlinear forcing singular vector-data assimilation (EnNFSV-DA) approach in the Zebiak-Cane model and used it for ENSO prediction, allowing the model to recognize the warm signal in the equatorial central Pacific eight months ahead (also see Yao et al. 2021). However, there is still significant uncertainty in the large coupled model in predicting and distinguishing ENSO types. It is urgently necessary to improve the prediction skill of El Niño diversity.

The season-dependent predictability barriers (PBs) significantly affect ENSO predictions, manifested as a sharp decrease in the prediction skill of models when predicting ENSO events during spring or summer (Webster and Yang

1992; Webster 1995; Zheng and Zhu 2010). Numerous studies have demonstrated that EP-El Niño predictions often suffer from spring PB (Yu et al. 2009; Duan and Wei 2013; Duan and Hu 2016; Qi et al. 2017). Recent studies have shown that the season-dependent PBs also affect CP-El Niño predictions but with different characteristics from the spring PBs in EP-El Niño predictions. Ren et al. (2016) indicated that the persistence barrier in two types of ENSO-related SSTA occurs in different seasons. The Niño3 SSTA has a spring persistence barrier, and the Niño4 SSTA has a summer persistence barrier. The season when the persistence barrier occurs is essentially associated with the occurrence of PB. To take a step further, Hou et al. (2019) examined the predictability of the two types of El Niño events separately by using multiple coupled model outputs. They revealed that summer PB often occurs in CP-El Niño predictions, while EP-El Niño predictions are mainly affected by spring PB.

The cause of PB has been investigated for many years. It is widely acknowledged that spring PB results from the combined effects of the annual climatological cycles, the structure of El Niño events, and particular initial error patterns (Mu et al. 2007a, b). This indicates that a particular initial error pattern can excite a PB for ENSO events. Therefore, the ENSO prediction skill can be improved by eliminating the initial uncertainty in key areas. To investigate the initial error patterns that have the most significant negative impact on the two types of El Niño, Tian and Duan (2016) tracked the evolution of nonlinear optimal perturbations (CNOP) in the Zebiak-Cane model. They concluded that the initial SST errors significantly impacting ENSO prediction are concentrated in the central and eastern tropical Pacific, highlighting the importance of tropical Pacific initial SST accuracy in distinguishing between El Niño types. Moreover, recent studies on the predictability of two types of El Niño have expanded the research region to the entire Pacific Ocean according to the ENSO mechanism associated with the extratropical factors. Vimont et al. (2014) indicated that the optimal initial conditions for CP ENSO events include warm SSTA in the northern subtropical Pacific area, while the optimal initial conditions for EP ENSO events include SSTA in the southern subtropical Pacific area. Hou et al. (2019) demonstrated that uncertainties in the North and Southeast Pacific are essential for predicting the structure and strength of different types of El Niño. Tseng et al. (2022) improved CP- and EP-El Niño predictability by incorporating extratropical precursors in the northern and southern hemispheres into models with existing tropical predictors, respectively.

As reviewed above, the two types of El Niño predictions are often limited by season-dependent PBs. CP-El Niño predictions are often influenced by the summer PB, while the spring PB is frequently found in EP-El Niño predictions.

Besides, not all CP(EP)-El Niño predictions tend to experience summer (spring) PBs. Some predictions of CP(EP)-El Niño also suffer from spring (summer) PBs. To the best of our knowledge, the research on the reason why two types of El Niño predictions tend to suffer from PB in different seasons is lacking. In addition, given the fact that specific initial errors from the Pacific can result in the occurrence of PBs in ENSO predictions, a question naturally arises: What kinds of initial errors lead to the varying season-dependent PBs in the two types of El Niño predictions? As such, in this paper, we manage to identify the initial errors most likely to lead to PBs occurring in different seasons for the two types of El Niño predictions and answer the following questions: (1) What are the differences in initial uncertainty from the tropical and extratropical Pacific Ocean trigger the summer PB for CP-El Niño but the spring PB for EP-El Niño? (2) How do these differences affect the seasonal variation of PBs for the two types of El Niño predictions? (3) Why does ENSO diversity make such a difference in the initial errors of the two types of El Niño predictions? These issues involve the dynamics of error growth. A novel approach to data analysis for ENSO predictability by using model output datasets proposed by Hou et al. (2019) is utilized. The details of the approach will be introduced in the following section.

The remainder of this paper is organized as follows. Section 2 presents the coupled model data outputs and introduces the methodology for ENSO predictability research in this study. In Sect. 3, we analyze the error evolution behavior and the phenomenon of seasonal-dependent PB for both types of El Niño. Section 4 compares the initial errors and their evolution leading to common season PB for both types of El Niño events. Section 5 analyses the effect of the initial error on the seasonal variation of PB for different El Niño separately and its plausibility. Finally, Sect. 6 includes a summary and discussion of the findings.

2 Data and an approach to data analysis for ENSO predictability

The CCSM4 model includes atmosphere, land, ocean, and sea ice components. The output of this model not only owns a good simulation of the real ocean, including the ability to simulate the spatial distribution and phase-locked behavior of ENSO (Ham and Kug 2014; Liu et al. 2021); Most importantly, the output of the CCSM4 model also can capture and distinguish the spatial modes of the two types of El Niño very well that it can simulate the El Niño diversity (Capotondi 2013; Feng et al. 2020; Freund et al. 2020). The ocean component of CCSM4 has a horizontal resolution of latitude/longitude with 320×384 points and 60 vertical

levels, while the atmospheric component has a horizontal resolution of latitude/longitude with 288×192 points and 28 vertical levels. Further information about CCSM4 can be found in Gent et al. (2011).

A novel method proposed by Hou et al. (2019) is applied, which can investigate climate system predictability dynamics from the initial error perspective only using model offline data. The mathematical proof of the method is introduced as follows. A state vector:

$$U(X, t) = [U_1(X, t), U_2(X, t) \dots U_n(X, t)], (X, t) \in \Omega \times [0, T]$$

where T denotes time, $T < +\infty$, $\mathbf{X} = (x_1, x_2, \dots, x_n)$, and its governing equations can be written as

$$\begin{cases} \frac{dU}{dt} = \mathbf{F}(U, t) + \mathbf{f} \\ U|_{t=0} = U_0 \end{cases}, in \Omega \times [0, T] \tag{1}$$

\mathbf{f} is the external forcing factor that is unchanged in the pi-Control runs, U_0 is the beginning state, and \mathbf{F} is a nonlinear operator. For a specific time, t_a to t_b ($t_a < t_b \leq T$), the integral form of Eq. (1) is

$$\begin{aligned} & \int_{t_a}^{t_b} dU - \int_{t_a}^{t_b} F(U, t) dt + \int_{t_a}^{t_b} f dt \\ & = \int_{t_a}^{t_b} F(U, t) dt + f(t_b - t_a) \end{aligned} \tag{2}$$

In this way, for the moment t_b , the corresponding state U_{t_b} can be written as

$$U_{t_b} = U_{t_a} + \int_{t_a}^{t_b} \mathbf{F}(U, t) dt + \mathbf{f}(t_b - t_a) \tag{3}$$

Similarly, two equations of the states U_{t_1} and U_{t_2} can be derived if we use two other time segments $[t_{01}, t_1]$ and $[t_{02}, t_2]$ with the same length.

$$U_{t_1} = \int_{t_{01}}^{t_1} \mathbf{F} dt + U_{t_{01}} + \mathbf{f}(t_1 - t_{01}) \tag{4}$$

$$U_{t_2} = \int_{t_{02}}^{t_2} \mathbf{F} dt + U_{t_{02}} + \mathbf{f}(t_2 - t_{02}) \tag{5}$$

Because the two time periods have the same time span, the difference between these two final states can be written as

$$U_{t_2} - U_{t_1} = U_{t_{02}} - U_{t_{01}} + \left(\int_{t_{02}}^{t_2} \mathbf{F} dt - \int_{t_{01}}^{t_1} \mathbf{F} dt \right) \tag{6}$$

The above Eq. (6) can be rewritten in the same form as Eqs. (4) and (5):

$$U_{t_2} - U_{t_1} = U_{t_{02}} - U_{t_{01}} + \int_{\Sigma} [F_{t_{02}} - F_{t_{01}}] dt \quad (7)$$

Herein, $F_{t_{02}}$ is F in Eq. (5), $F_{t_{01}}$ is F in Eq. (4), and $\int_{\Sigma} [F_{t_{02}} - F_{t_{01}}] dt$ represents the difference between the integral of $F_{t_{02}}$ over $[t_{02}, t_2]$ and the integral of $F_{t_{01}}$ over $[t_{01}, t_1]$. Equation (7) implies that the difference between U_{t_1} and U_{t_2} is only a matter of the initial difference of $U_{t_{02}} - U_{t_{01}}$. That is, the difference between U_{t_1} and U_{t_2} can be thought of as being derived by the model Eq. (3) with the initial difference $U_{t_{02}} - U_{t_{01}}$ (see Fig. 1). If we assume the integration in the time segment $[t_{01}, t_1]$ to be an observation and the other one in the time segment $[t_{02}, t_2]$ to be a prediction of that observation, the difference between the initial states of these two time segments is the initial error and that between the final states of these two time segments is the prediction error. Therefore, Eq. (7) indicates that the prediction error is only caused by the initial error. Emphasis should be placed on the fact that this data-analysis method can only be used in analyzing climate or weather variability associated with a climatological cycle, namely the annual cycle or diurnal cycle. In addition, t_{01} and t_{02} should be at the same corresponding moments in different cycles. In this study, the predictability dynamics of El Niño events, which

have interannual periodic variations, are explored. Additionally, t_{01} and t_{02} correspond to January in different years, while t_1 and t_2 correspond to December in different years.

Based on the above considerations, 13 typical EP-El Niño years and 13 typical CP-El Niño years are selected from the 500-year integral of CCSM4 model output data and are regarded as “observation” years. The criteria for selecting EP-(CP-) El Niño is following Kug et al. (2010), we use Niño3 and Niño4 SSTA [i.e., the SST anomaly averaged over the Niño3 area (150°E–90°W, 5°S–5°N) and that over the Niño4 area (150°E–90°W, 5°S–5°N)] to measure the intensities of EP and CP-El Niño, respectively. Generally, it is regarded as a typical EP- (CP-) El Niño when the related Niño3 (Niño4) SSTA greater than 0.5 persists at least 6 months and peaks in the boreal winter (NDJ). These typical El Niño events have good phase-locking, which turns warm in the early boreal spring and peaks at the end of the year (Fig. 2). For each one-year “observation”, the corresponding 40 one-year segments around this certain year are selected to fabricate 40 “predictions” for this “observation” with a 12-month lead time. In this way, 520 predictions in total for these CP and EP-El Niño events are obtained. Then, the prediction error $E(t)$ can be expressed as follows.

$$E(t) = \sqrt{\frac{1}{N} \sum_{(i,j)} [T_{(i,j)}^p(t) - T_{(i,j)}^o(t)]^2} \quad (8)$$

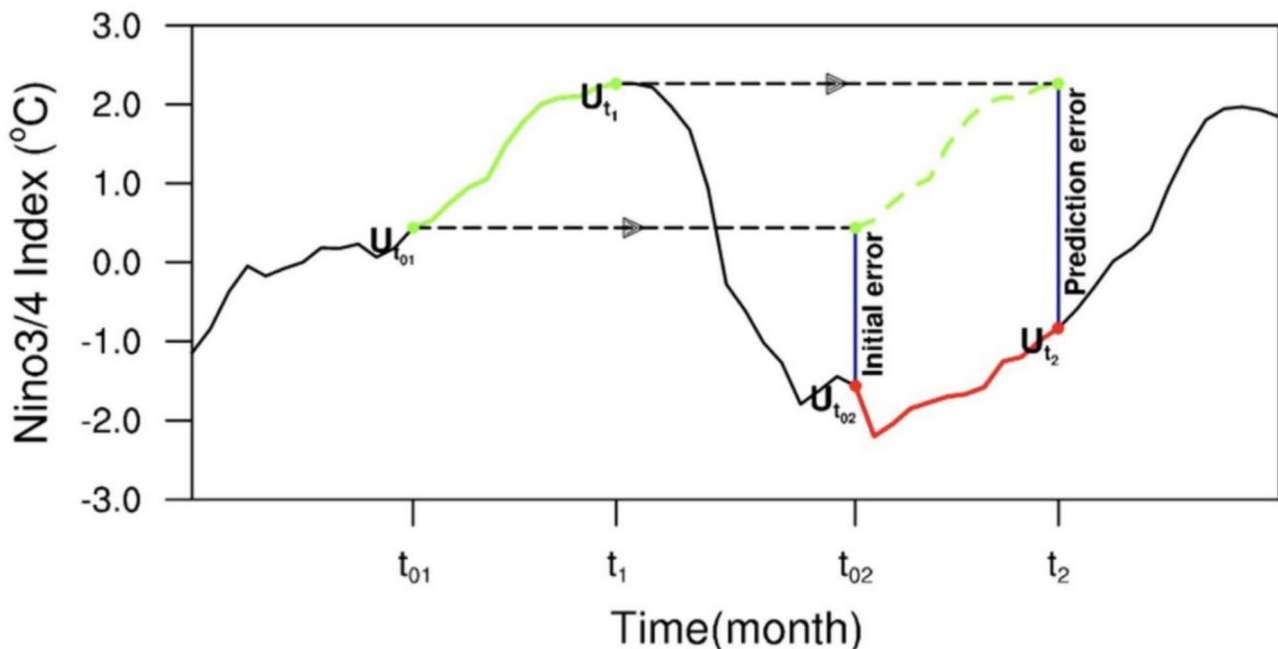


Fig. 1 Schematic diagram of the approach to data analysis for predictability. The black solid curve denotes the time-dependent pi-Control run of SST. Two one-year time periods are picked, as denoted by the green and red curves. The SST time series during the time period $[t_{02}, t_2]$ is moved to $[t_{02}, t_2]$ fit that during. If the former SST time

series is regarded as an “observation”, the latter SST time series can be thought of as a “prediction” of that “observation”. The corresponding initial error and prediction error are represented by the SST difference between t_{02} and t_{01} and between t_2 and t_1 , which are marked by the two navy blue lines. From Fig. 1 in Hou et al. (2019)

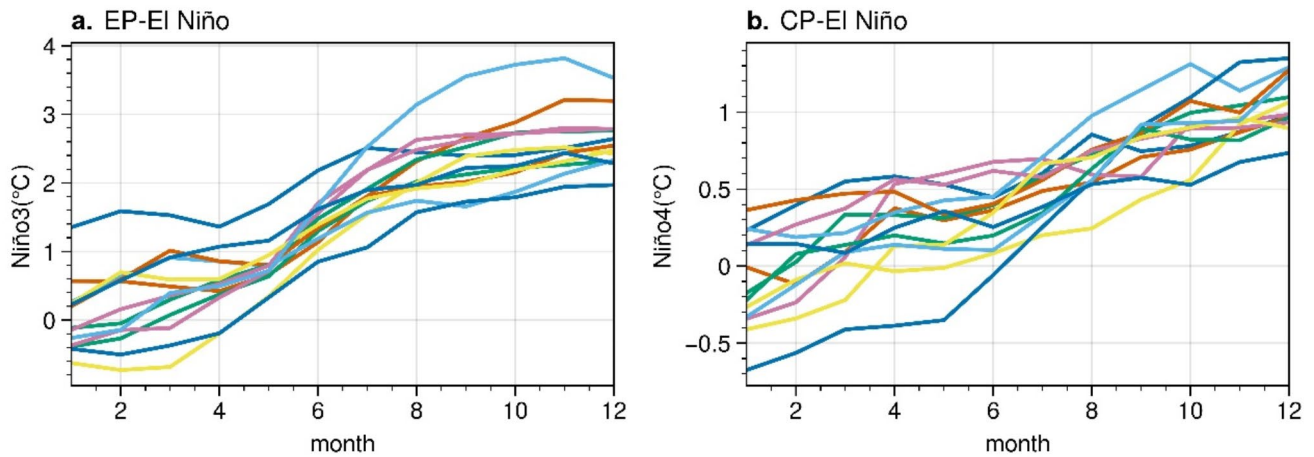


Fig. 2 Niño3 index (a unit: °C) for the 13 selected EP-El Niño events and Niño4 index (b, unit: °C) for the 13 selected CP-El Niño events over time

where T^P stands for “prediction”, T^o stands for “observation”, (i, j) stands for grid points, and N stands for the total number of grid points in the Niño4/ Niño3 region for CP-El Niño/EP-El Niño predictions.

The PBs for the two types of El Niño is distinguished by measuring the prediction error growth trend proposed by Mu et al. (2007a). Since we use the monthly data derived from the model outputs, the prediction error growth trend can be expressed as the slope κ of the curve $E(t)$, which can be approximated as $\kappa \approx \frac{E(t_0+\Delta t)-E(t_0)}{\Delta t}$, with Δt being 1 month. The positive (negative) value of κ represents the trend of increasing (decreasing) prediction error for the month. The larger the absolute value of κ , the faster the rate of increasing or decreasing of the prediction error. Then the prediction error growth rate for a season can be expressed as the sum of three successive months in that season. A significant maximum value of κ for a particular season implies the fastest growth of prediction error occurs, indicating the occurrence of PB in that season.

3 Error evolution behavior and seasonal-dependent PBs phenomenon for two types of El Niño events

As previously mentioned, we acquired 520 predictions for the 13 CP-El Niño and 13 EP-El Niño events individually by using CCSM4 data outputs. To investigate the distinct characteristics of the seasonal-dependent PBs for two types of El Niño predictions, the error growth behavior is explored for each type individually. Figure 3 displays the monthly growth rates of the prediction errors in Niño3 (Fig. 3a) and Niño4 (Fig. 3b) SSTA components for the 520 predictions of EP- and CP-El Niño. The CCSM4 model

reasonably simulates and distinguishes the seasonal dependence of error growth in the predictions of the two types of El Niño events. The monthly prediction error growth rates of the Niño3 SSTA reach their maximum value from May to June for most EP-El Niño predictions. In contrast, the monthly prediction errors of the Niño4 SSTA increase more rapidly in June-September for most CP-El Niño predictions. These findings suggest that most CP-El Niño predictions are affected by summer PB, while EP-El Niño predictions are primarily affected by spring PB.

It is worth noting that not all 520 EP(CP)-El Niño predictions exhibit PB solely during spring (summer). In some cases, PB occurs during other seasons but is less common. Figure 4 depicts the error evolution of the related Niño SSTA in EP- and CP-El Niño predictions with spring and summer PB. Errors in all these predictions show general trends of decrease in the first period followed by significant increases in a particular season. Therefore, the PB occurs during the season when the corresponding errors grow rapidly. Besides, summer PB can occur in certain predictions of EP-El Niño. However, it is evident that the initial errors triggering spring PB tend to cause larger prediction errors in December compared to the one causing summer PB, on average (Fig. 4a). This implies that spring PB is more likely to happen and have a more significant effect on EP-El Niño predictions. Likewise, although some CP-El Niño predictions may suffer from spring PB, the initial error that causes summer PB tends to result in larger initial errors in December (Fig. 4b). Therefore, summer PB has a more considerable impact on CP-El Niño predictions than spring PB.

As illustrated in the previous section, the prediction error is only determined by the initial error. The difference when PB occurs also comes from the difference in the initial error. What differences in the initial errors affect the varying season-dependent PB in the two types of El Niño predictions?

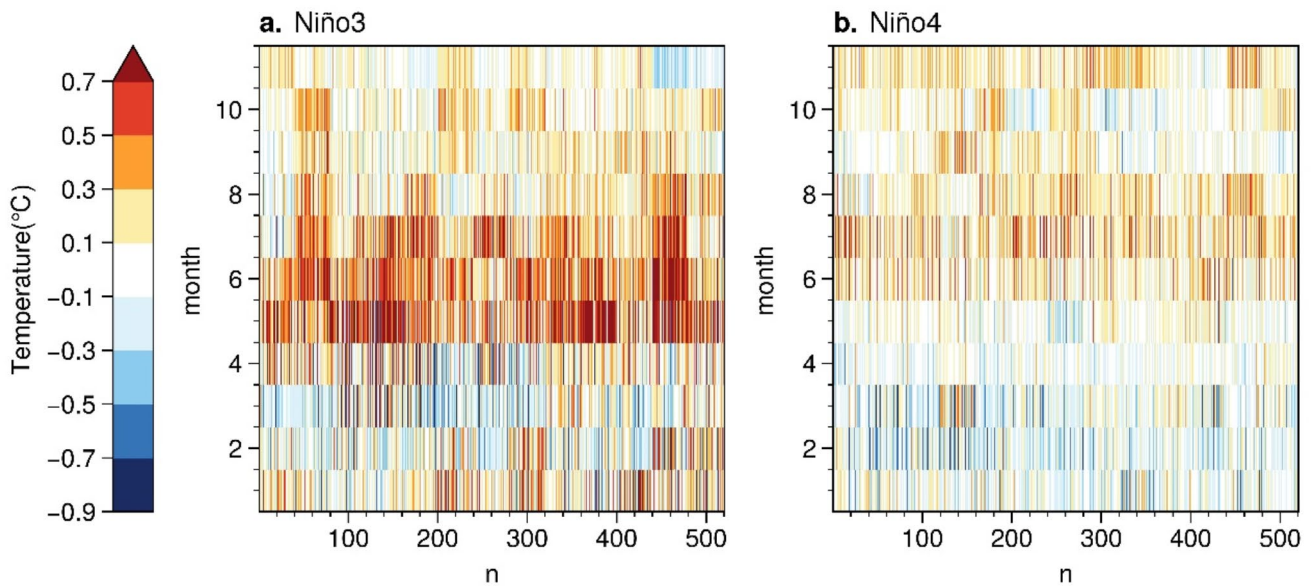


Fig. 3 Monthly prediction error growth rates for 520 Niño3 (a) and Niño4 (b) SST predictions. The horizontal axes denote the sample of prediction, and the vertical axes represent the calendar month. Red

(blue) shading indicates that the prediction has a positive (negative) error growth rate in that month, with an increasing (decreasing) trend

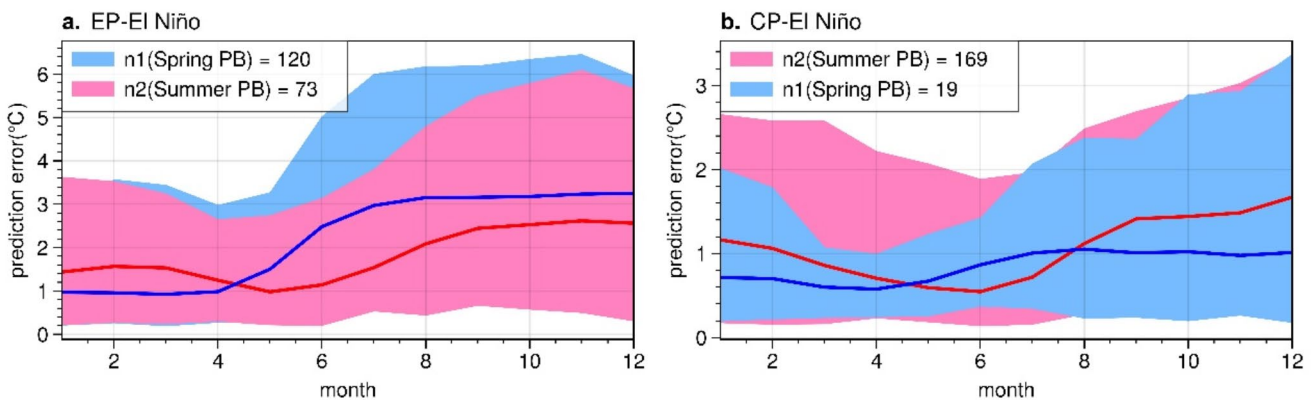


Fig. 4 SSTA Error evolution of 520 predictions in Niño3 (a) and Niño4 (b) region over time. The blue (pink) shaded region represents the error evolution of spring (summer) PB cases. The blue line (red line) represents the ensemble average of the individual errors for PB occur-

rences in spring (summer). The inset in the upper left corner denotes “n1” (“n2”), which represents the number of cases of spring (summer) PB in the predictions for two types of El Niño

In addition, how do these initial errors evolve and affect PB occurrence?

4 Initial errors resulting in spring PB for EP-El Niño and Summer PB for CP-El Niño and their evolutionary mechanism

The conclusion drawn from the previous section is that EP-El Niño is more susceptible to spring PBs, whereas CP-El Niño is mainly affected by summer PBs. To investigate the initial errors that are most likely to result in spring PB for EP-El Niño and summer PB for CP-El Niño, as well as the

pattern of error evolution. All EP-El Niño predictions that trigger spring PB and all CP-El Niño predictions that trigger summer PB are selected and denoted as EP-spring-PB-predictions and CP-summer-PB-predictions individually, the numbers of which are presented in Fig. 4. An Empirical Orthogonal Function (EOF) analysis is conducted on the initial errors in the two types of predictions over the Pacific region [66.5°S–66.5°N, 120°E–70°W]. The first EOF mode of EP-spring-PB-predictions accounts for approximately 22.6% of the total variance of the initial errors, and that of CP-summer-PB-predictions accounts for approximately 28.3% of the total variance of the initial errors, which is well dominant that 2nd (11.7% and 8.8%) and 3rd (10.5%

and 7.5%) mode. These two first modes can reflect the primary spatial structural characteristics of these initial errors. Using the first EOF mode as a basis, the initial errors highly correlated with the first EOF modes are selected. Specifically, if the projection coefficient (PC) value is greater than the mean of the positive PC values for all initial errors, the corresponding initial error can be regarded as highly positively correlated with this EOF mode. On the contrary, the PC value lower than the mean of negative PC values for all initial errors is regarded as highly negatively correlated with this mode. For initial errors leading to spring PB in EP-El Niño predictions and summer PB in CP-El Niño predictions two groups denoted as EOF1+ and EOF1- are divided based on the sign of the correlation coefficient with the first EOF mode. We discovered that for both spring and summer PB-related initial errors, the initial errors in the EOF1- group resulted in more pronounced PB phenomena and stronger prediction errors than the EOF1+ group. Therefore, we concluded that the initial errors in the EOF1- group have a greater impact on both spring PB for EP-El Niño predictions and summer PB for CP-El Niño predictions. For ease of explanation, we refer to the initial errors in the EOF1- groups that lead to spring PB for EP-El Niño and summer PB for CP-El Niño as EP-spring-type initial errors and CP-summer-type errors respectively, which are obtained after synthetic averaging of the EOF1-group errors, and are not specific to a particular individual case. These errors include the ocean temperature and horizontal wind components.

Figure 5a and b show the spatial structures of EP-spring-type and CP-summer-type initial errors. To compare their differences more intuitively, the distinct distributions of CP-summer-type minus EP-spring-type are also presented in Fig. 5c. The overall distribution of the two types of errors has a similar structure. The SST error shows a negative-positive-negative-positive error characteristic along the direction of the northwest Pacific-tropical eastern Pacific-southeastern Pacific. Both EP-spring-type and CP-summer-type errors over the tropics display a dipole pattern, with negative error anomalies in the western sub-surface Pacific primarily concentrated between 95 and 135 m and positive error anomalies in the upper layer of the eastern tropical Pacific. In the northeast Pacific, two types of errors show strong anomalies above 55 m, with negative anomalies near the northwest of Midway Island and positive anomalies around the Gulf of Alaska. This North Pacific error pattern resembles the Victoria Mode (VM-like mode) proposed by Chiang and Vimont (2004) and Ding et al. (2015). Over the southeastern Pacific, EP-spring-type and CP-summer-type errors have dipole sea surface temperature (SST) with negative error anomalies in the southwest and positive error anomalies in the northeast, resembling the South Pacific

meridional mode (SPMM-like mode) proposed by Bond et al. (2003) and Min et al. (2017).

Figure 5c shows the differences in initial errors between EP-spring-type and CP-summer-type, highlighting that the two types of initial errors are primarily characterized by differences in intensity of error anomaly. The largest difference zone is in the tropical Pacific, where CP-summer-type exhibits stronger positive error anomalies of initial error from the surface to a depth of 135 m in the equatorial eastern Pacific and stronger negative anomalies of initial error in the subsurface layer of the equatorial western Pacific compared to the EP-spring-type errors. Additionally, slightly stronger positive anomalies of the VM-like mode error are observed for CP-summer-type than EP-spring-type error in the extratropical Pacific. Overall, these differences in initial error patterns may contribute to the seasonal variation in PB occurrence in EP- and CP-El Niño predictions. Then, how does this difference affect the evolution of the two types of initial errors, ultimately leading to the PB in the EP-El Niño predictions occurring during the spring and the PB in the CP-El Niño predictions occurring during the summer?

By tracing the evolution of EP-spring-type and CP-summer-type initial errors (Figs. 6 and 7), it is found that these two types of initial errors exhibit similar evolutionary behaviors. They initially exhibit an El Niño-like decaying trend, which then transitions to the growth phase of a canonical La Niña-like event, ultimately resulting in a cold bias of the SST with a cold center in the tropical central-eastern Pacific by December. From a physical perspective, positive SST errors over the middle-eastern equatorial Pacific in EP-spring-type and CP-summer-type errors induce strong westward winds over the middle-eastern equatorial Pacific, resulting in the westward propagation of Rossby waves. Upwelling Kelvin waves are induced once the Rossby waves reach the western ocean boundary, propagating eastward and upward. The strong lower-level negative anomalies in the equatorial western Pacific lift towards the surface layer of the tropical eastern Pacific, causing the positive anomalies in the surface layer of the tropical eastern Pacific to offset gradually. Once the positive SST errors in the equatorial eastern Pacific disappear and negative SST errors appear, eastward wind anomalies will be generated, and the cooling process gradually expands westward under the Bjerknes positive feedback mechanism, resulting in a cold error bias over the tropical Pacific Ocean in December.

The primary difference in error evolution between the two types of errors lies in the season of the positive-to-negative phase transitions of SST anomalies over the tropical central-east Pacific. EP-spring-type initial errors undergo this transition around March-April (spring), while CP-summer-type initial errors undergo it around May-June (summer). The correspondence between the seasons of the

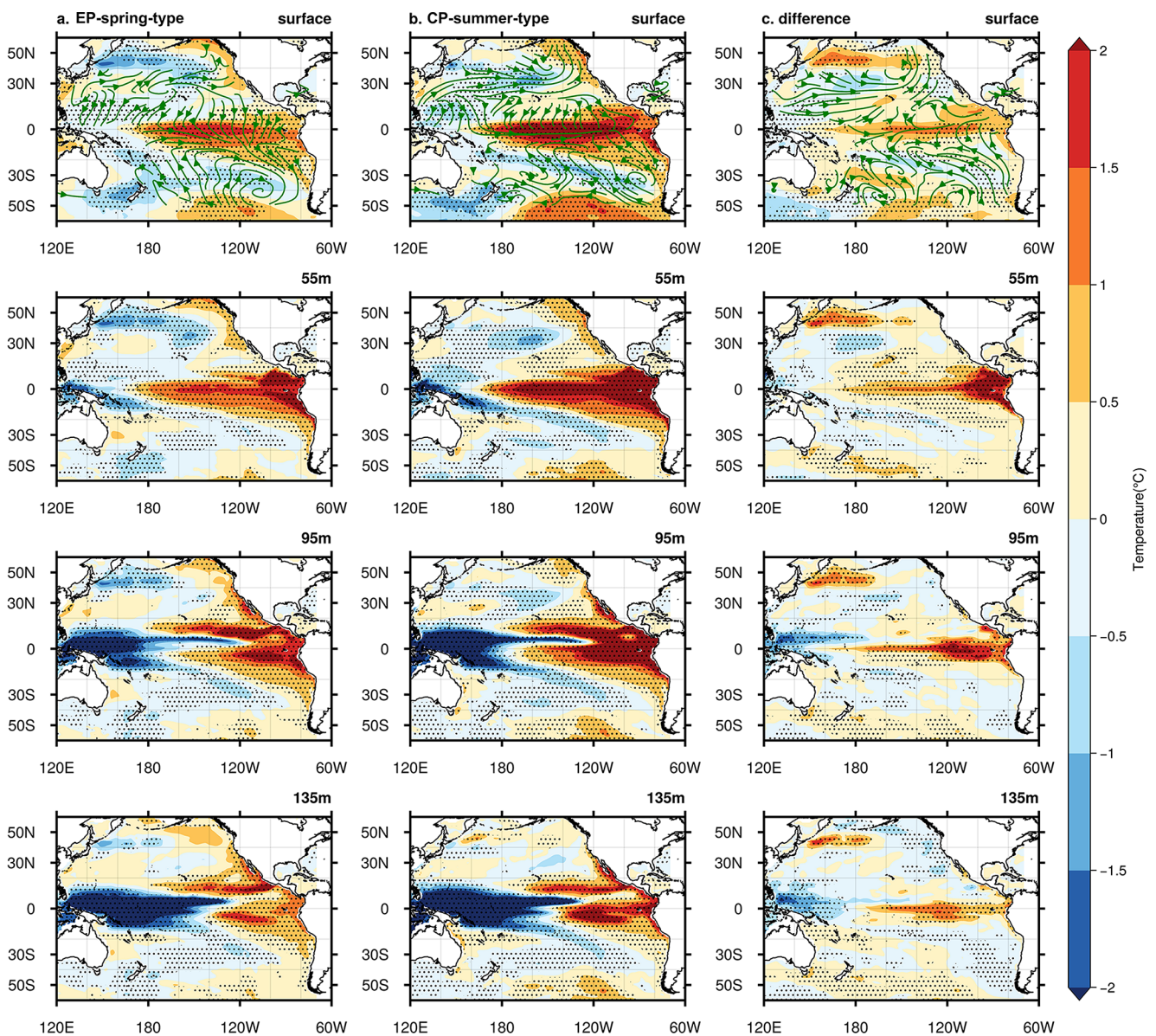


Fig. 5 EP-spring-type (column **a**) and CP-summer-type (column **b**) initial errors in Pacific ocean temperatures and surface winds, and their difference from each other (CP-summer-type minus EP-spring-type,

column **c**). Rows 1–4 indicate different ocean depths: 0 m, 55 m, 95 m, 135 m. The initial error of the dotted area in the figure passes the 95% significant t-test

positive-to-negative transitions phase of SST error over the tropical central-east Pacific and the season of PB occurrence gives reason to speculate about the link between these two phenomena. So further, we find that the evolution of EP-spring-type /CP-summer-type initial errors explains well the trend of decreasing and then increasing the error in the Niño3/4 region for the EP/CP-El Niño predictions in Fig. 4. During the pre-El Niño-like recession period, the positive SST error in the tropical central-east Pacific undergoes a continuous decrease to complete disappearance due to the neutralizing effect, which aligns with the observed decline to their lowest points in the SST error in the Niño3/4 region (Fig. 4). Subsequently, the negative error expands and

intensifies in the westward direction, resulting in a period of rapid growth in the SST error in the Niño3/4 region (Fig. 4), which means that PB is beginning to occur. Therefore, the positive and negative phase transition of the SST error over the central-eastern tropical Pacific corresponds to the shift of the error in the Niño3/4 region bottoming out and then rebounding in Fig. 4. It can be concluded that the onset of PB occurrences often occurs during the transition from positive to negative of the initial error evolution in the east-central tropical Pacific.

The amplitude difference of positive SST error between EP-spring-type and CP-summer-type initial errors over the North Pacific VM region and the east-central tropical Pacific

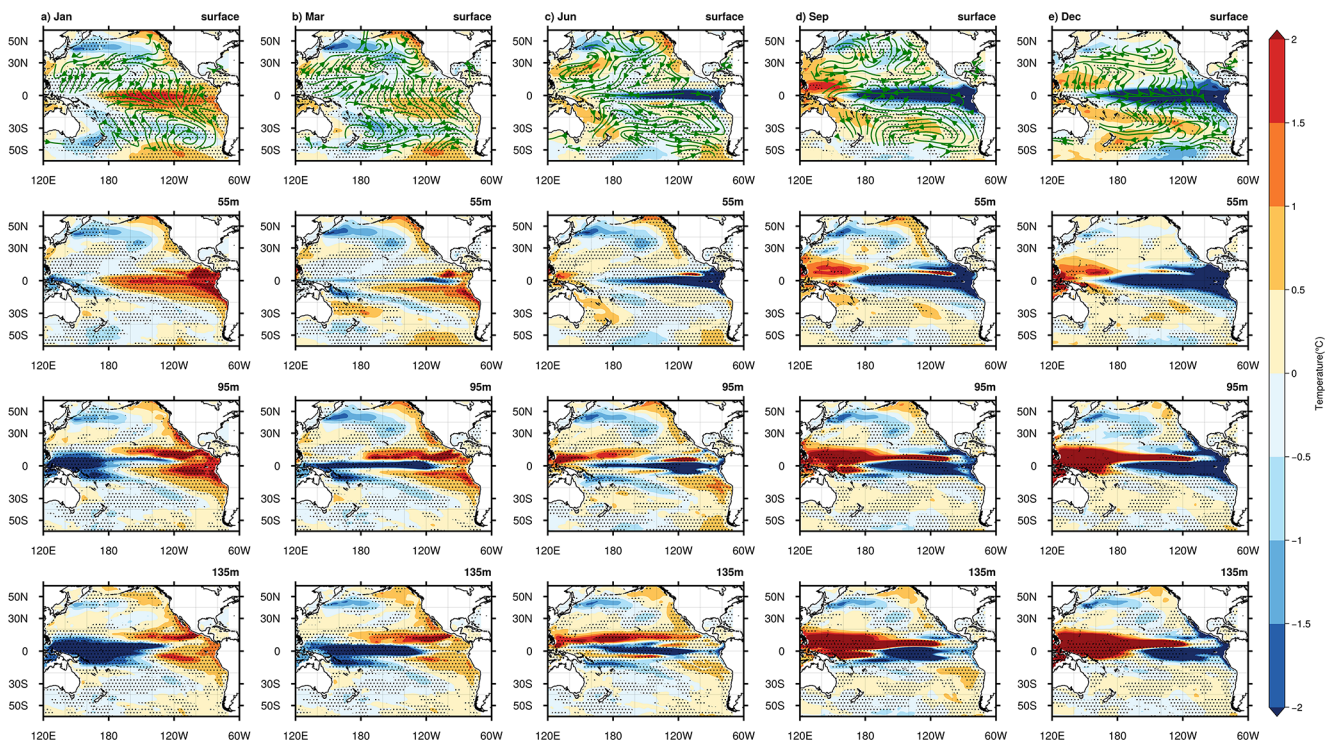


Fig. 6 EP-spring-type sea temperature (unit: °C) and sea surface wind field (unit: m/s) initial error in (a) January, (b) March, (c) June, (d) September, (e) December. Each row represents an ocean depth of 0 m, 55 m, 95 m, and 135 m from top to bottom. The dotted area in the figure passed the 95% significant t-test

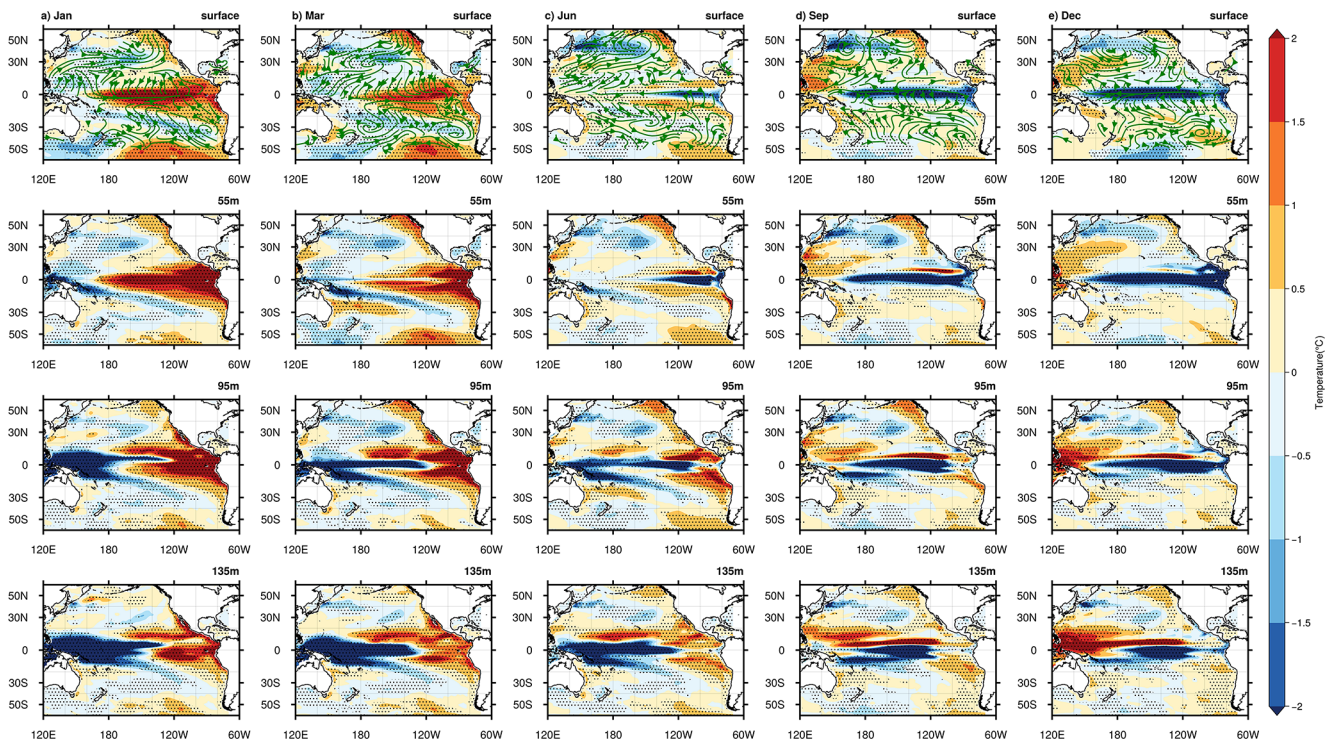


Fig. 7 As in Fig. 6, but for CP-summer-type error

has a notable influence on the error evolution, as illustrated in Fig. 8. In comparison to the initial EP-spring-type error, the initial CP-summer-type error exhibits much stronger positive SST error anomalies over the equatorial eastern Pacific, resulting in negative error anomalies from the subsurface of the western equatorial Pacific taking much longer to fully neutralize to eliminate the positive error anomalies. Thus negative error are not observed until June (early summer) for CP-summer-type initial errors, while EP-spring-type errors produce negative SST anomalies as early as April (early spring). This phenomenon suggests that stronger initial SST error over the equatorial eastern Pacific will delay the onset of PB in the predictions. Regarding the impact of initial errors over the extratropical ocean, CP-summer-type initial errors in the northeastern Pacific from January to June show slightly stronger positive VM-like errors compared to EP-spring-type initial errors, although not as significant as in the equatorial Pacific, which have a particularly strong influence on the tropics through wind-evaporation-SST (WES) feedback (Xie and Philander 1994). This implies that a positive SST error along the Gulf of Alaska can cause a local convective anomaly. This, in turn, triggers an oblique pressure response in the atmosphere, resulting in anomalous southwesterly winds over the positive SST anomaly. As a result, the prevailing northeasterly trade winds in the background field weaken, and latent heat release reduces. The anomalous wind will direct the positive SST anomaly to lower latitudes, thus suppressing the formation of cold anomalies in the equatorial Pacific. Therefore, the positive-to-negative phase transitions of the tropical SST anomaly are delayed during the evolution of the CP-summer-type initial error, and the PB appears later.

Based on the above results, it can be concluded that the onset of PB often occurs during the phase transition from positive to negative of the initial error evolution in the central eastern tropical Pacific. In addition, the CP-summer type initial errors exhibit stronger positive error anomalies in the tropical Pacific and VM region in the northeastern extratropical Pacific compared to the EP-spring-type. These stronger positive initial errors evolve to postpone the phase transition of the error in the central eastern tropical Pacific from positive to negative, thus triggering the occurrence of the summer PB for CP-El Niño, rather than the common spring PB for EP-El Niño.

5 Analysis of the initial errors affect the PB seasonal variation for CP- and EP- El Niño

Section 4 has elucidated and compared the initial errors that most likely trigger the common occurrence of spring PB for EP El Niño and summer PB for CP El Niño predictions individually. Besides, it has been found in Sect. 3 that summer PB and spring PB also occur in some EP-El Niño and CP-El Niño prediction cases, although they cause weaker prediction errors in December and are less common. Therefore, we naturally wonder whether the unique characteristics in initial errors causing the spring PB for EP-El Niño and the summer PB for CP-El Niño in Sect. 4 also appear in the seasonal variation of PB occurring in the same type of El Niño predictions. Specifically, it is the stronger positive initial errors in the tropical Pacific and the VM region in the northeastern extratropical Pacific that hold back the phase transition of the error in the central-eastern tropical Pacific,

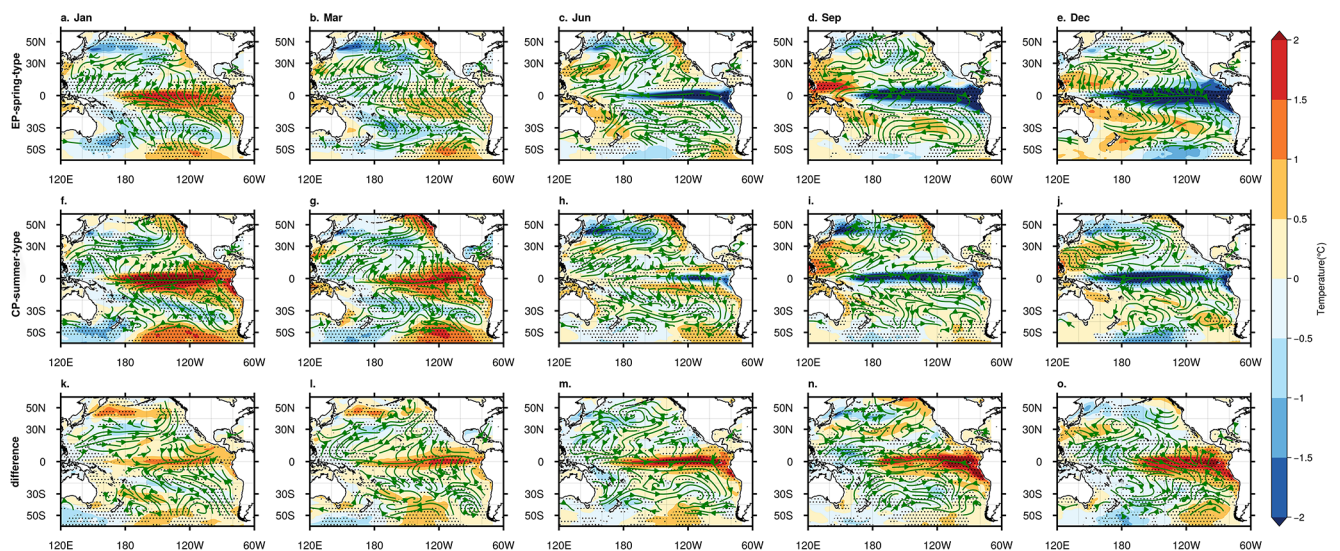


Fig. 8 EP-spring-type (first row) and CP-summer-type (second row) error evolution of SST (unit: °C) and sea surface wind field (unit: m/s) in (a) January, (b) March, (c) June, (d) September, (e) December, and

difference between (CP-summer-type minus EP-spring-type, third row). The dotted area in the figure passed the 95% significant t-test

triggering summer PB for CP-El Niño when comparing the evolution of the EP-spring-type and CP-summer-type initial errors. Is it the same situation when comparing the initial errors causing spring PB and summer PB for one single type of El Niño prediction?

We first explore what initial errors can cause spring PB for CP-El Niño (denoted as CP-spring-type initial errors) and compare it with CP-summer-type and EP-spring-type initial errors. The study aims to figure out whether is it still the initial error in the central-eastern tropical Pacific and VM region in the northern Pacific that affects the seasonal variation of PB occurrence for CP-El Niño. As the initial errors that both trigger springs PBs, are there any common features between CP-spring-type and EP-spring-type initial errors? To investigate the initial errors that are most likely to result in spring PBs in CP-El Niño predictions, all predictions for CP-El Niño that trigger spring PB are selected and denoted as CP-spring-PB-predictions, the number of which are presented in Fig. 4b. Similar to the pathway for obtaining CP-summer-type initial errors. An EOF analysis is conducted on the initial errors in the CP-spring-PB-predictions over the Pacific region [66.5°S–66.5°N, 120°E–70°W]. The first EOF mode of CP-spring-PB-predictions accounts for approximately 25.3% of the total variance of the initial errors. Using the first EOF mode as a basis, the initial errors highly correlated with the first EOF modes are selected. Its selection criteria were consistent with those in Sect. 4 based on the sign of the correlation coefficient with the first EOF mode classifying it into two groups that are highly positively and negatively correlated with this mode, the EOF+ and EOF- groups respectively. We discovered that for CP-spring-related initial errors, the initial errors in the EOF1- group resulted in more pronounced PB phenomena and stronger prediction errors than the EOF1+ group. Therefore, we concluded that the initial errors in the EOF1- group have a greater impact on spring PB for CP-El Niño predictions, we call the initial error of the EOF1- group leading to the spring PB of CP-El Niño the CP-spring-type initial error. These errors include the ocean temperature and horizontal wind components.

Figure 9a and b show the spatial structures of CP-spring-type and CP-summer-type initial errors. To compare their differences more intuitively, the distinct distributions of CP-summer-type minus CP-spring-type are also presented in Fig. 9c. CP-spring-type and CP-summer-type share similar pattern in the equatorial and South Pacific, both exhibit a subsurface temperature dipolar structure with positive error in the central-eastern equatorial Pacific and negative error in the lower layers of the western equatorial Pacific, as well as SPM-like initial errors in the south Pacific. In addition to the similarity of the error patterns in the tropical and South Pacific, their error strengths are comparable, and the

magnitude of the initial positive SST errors in the tropical Pacific does not have the differences described in the comparison of the EP-spring-type and CP-summer-type errors in Sect. 4.

The most significant difference between the two types of initial errors is over the northern Pacific. Unlike the significant VM-like mode error of the CP-summer-type initial errors, the CP-spring-type error does not show any significant structure in the northern Pacific. This characteristic is quite similar to the EP-spring-types (Fig. 5a). That means neither type of error that gives rise to spring PB has a significant positive error in the northeastern Pacific. Furthermore, it implies that the seasonal variation of PB occurring in CP-El Niño prediction is sensitive to the initial errors in the North Pacific by comparing the CP-spring-type and CP-summer-type errors. Then, is this difference between CP-spring-type and CP-summer-type initial errors in the northern Pacific responsible for the PB seasonal variation in CP-El Niño predictions?

By tracing the evolution of CP-spring-type (Fig. 10) and CP-summer-type (Fig. 7) initial errors, it is found that these two types of initial errors exhibit similar evolutionary behaviors. They first experience a decaying period of El Niño, and then a transition to a central La Niña-like mode in April-May-June. This transition triggered a cold bias of predictions in the central-eastern equatorial Pacific in December. The physical mechanism behind this is that the positive errors in the central and eastern Pacific promote strong westerly winds in the equatorial Pacific, which generate westward-propagating Rossby waves. Once these Rossby waves reach the western boundary, they trigger eastward-propagating Kelvin waves of upwelling. These Kelvin waves gradually bring the negative anomalies in the lower western equatorial Pacific upward and eastward to the sea surface, offsetting the positive sea surface temperature anomalies in the central and eastern Pacific. This dissipation process of the positive error anomalies corresponds to the pre-declining trend of the error in the Niño4 region in Fig. 4b. The appearance of negative SST error in the eastern Pacific forms a Bjerknes positive feedback mechanism, which extends the negative SST error westward, thus producing a large cold bias in the upper east-central Pacific Ocean in December. The continued expansion of the negative error explains the trend of rapid growth of error in the later stages in Fig. 4b and implies that PB is in progress.

As shown in Fig. 11, the initial positive SST errors over the central-eastern equatorial Pacific are significantly faster to dissipate during the evolution of the CP-spring-type errors than the CP-summer-type errors. The key to the different rates of error evolution is the difference in two types of initial errors over the northern Pacific Ocean for CP-El Niño predictions. Compared to the CP-spring-type error, the

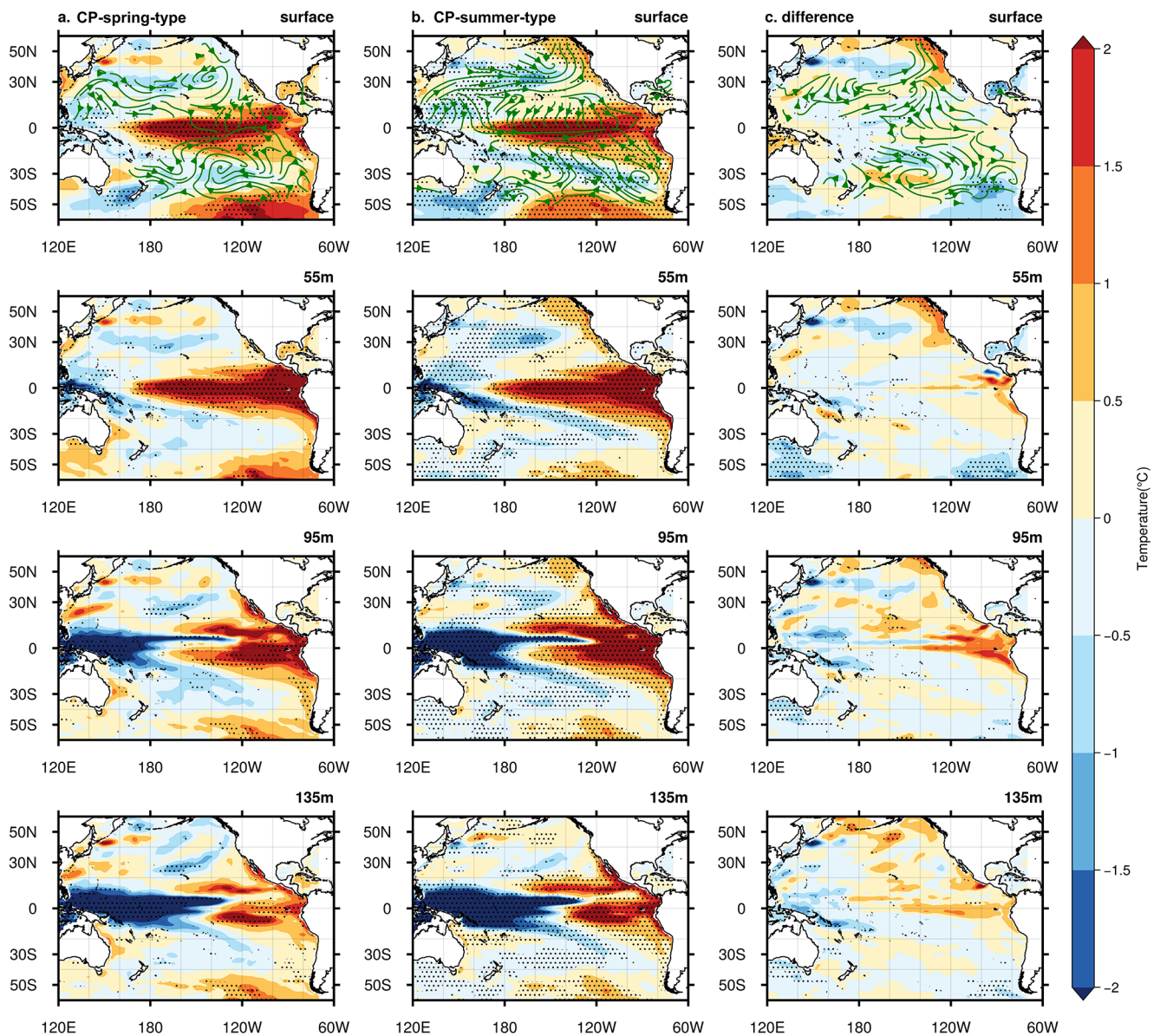


Fig. 9 CP-spring-type (column a) and CP-summer-type (column b) initial errors in Pacific ocean temperatures and surface winds, and their difference from each other (CP-summer-type minus CP-spring-type,

column c). Rows 1–4 indicate different ocean depths: 0 m, 55 m, 95 m, 135 m. The initial error of the dotted area in the figure passes the 95% significant t-test

CP-summer-type exhibits a stronger positive VM-like error over the northeast Pacific from January to June, which has a particularly strong influence on the deep tropics through WES feedback. That is, the VM-like warm error component located in the upper layers of the northeast Pacific Ocean can induce the atmosphere to generate diagonal pressure effects. This leads to the formation of southwesterly wind anomalies that move in the opposite direction of the northeasterly trade winds of the background field. Consequently, the latent heat fluxes get suppressed, preventing heat release, and causing the positive SST error anomalies of the northeast Pacific Ocean to propagate towards lower latitudes, which leads to the positive SST error in the central-eastern tropical Pacific

persisting much longer than those no VM-like mode error. These prolonged positive SST errors delay the transition from positive to negative SST error in the tropical Pacific, and the negative SST error in the equatorial Pacific naturally emerges much later, thus leading to a delay in PB as well. In summary, the VM-like modes in initial error over the northern Pacific are the major reason influencing the occurrence of summer PB rather than spring PB for CP-El Niño. This conclusion reiterates the point raised in Sect. 4 about the importance of VM regional errors in influencing seasonal variation of PB and is consistent with the points drawn by many studies that NPO-forced VM mode is closely

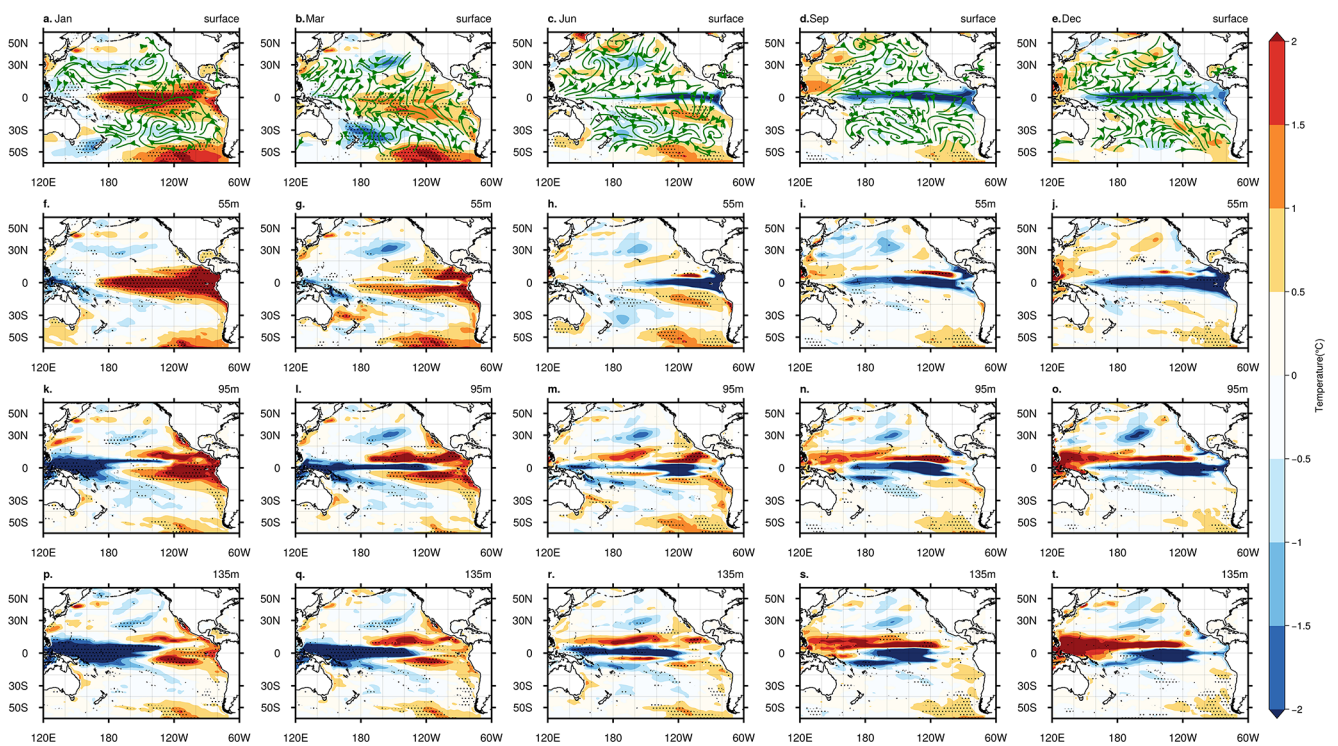


Fig. 10 CP-spring-type sea temperature (unit: °C) and sea surface wind field (unit: m/s) initial error in (a) January, (b) March, (c) June, (d) September, (e) December. Each row represents an ocean depth of 0 m, 55 m, 95 m, and 135 m from top to bottom. The dotted area in the figure passed the 95% significant t-test

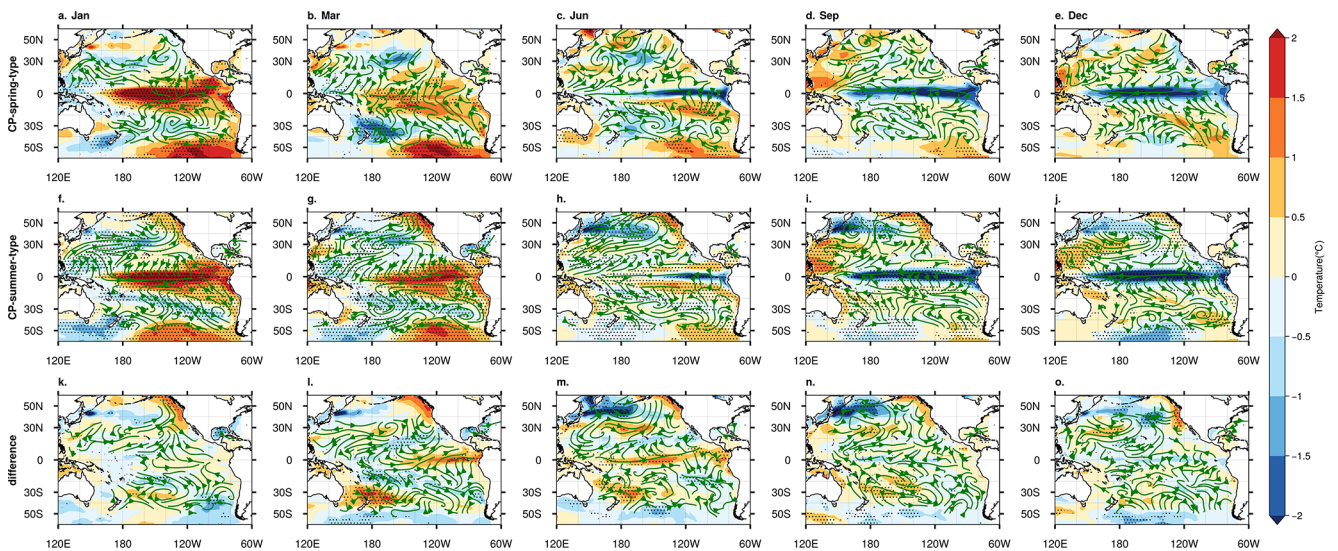


Fig. 11 CP-spring-type (first row) and CP-summer-type (second row) error evolution of SST (unit: °C) and sea surface wind field (unit: m/s) in (a) January, (b) March, (c) June, (d) September, (e) December, and difference between (CP-summer-type minus CP-spring-type, third row). The dotted area in the figure passed the 95% significant t-test

associated with the CP El Niño based on observation and model results (Yeh et al. 2015; Wang et al. 2019b).

For the EP-El Niño, it is mentioned in Sect. 3 that most predictions interfere with spring PB, and some certain cases are suffering from summer PB. To investigate whether the initial error in the central-eastern Pacific and North Pacific

VM region influences the seasonal variation of PB in EP-El Niño, we obtain the EP-summer-type error through a similar pathway for identifying EP-spring-type error. It is shown that the EP-summer-type initial errors (Fig. 12b) share a structural resemblance with EP-spring-type initial errors (Fig. 12a), which have been described in Sect. 4. Although

the amplitude of positive errors is comparable in the northeast Pacific for the two types of initial error, there are still differences in the strength of the errors in some regions. (As shown in Fig. 12c). The most important region to be focused on is the central-eastern tropical Pacific, where EP-summer-type exhibits stronger positive error from the surface to a depth of 135 m in the eastern tropical Pacific and stronger negative error in the subsurface layer of the western tropical Pacific compared to the EP-spring-type errors.

Figure 13 shows that EP-summer-type errors evolve similarly to EP-spring-type errors (Fig. 9). Specifically, the initial warm bias of the errors gradually transitions into a

cold phase in the east-central equatorial Pacific, eventually triggering a cold bias in December (13e). As explained above, the occurrence time of PB is also decided by the early or late onset of the SST phase transition in the tropical Pacific. By comparing the evolution of EP-summer and spring-type errors across months (Fig. 14), the role of the aforementioned error regions in influencing the rate of error evolution for EP-El Niño is identified. Compared to the EP-spring-type initial error, the EP-summer-type initial error exhibits much greater amplitudes of the positive SST error in the central-eastern Pacific, leading to a slower dissipation of positive error and a later show-up of negative error

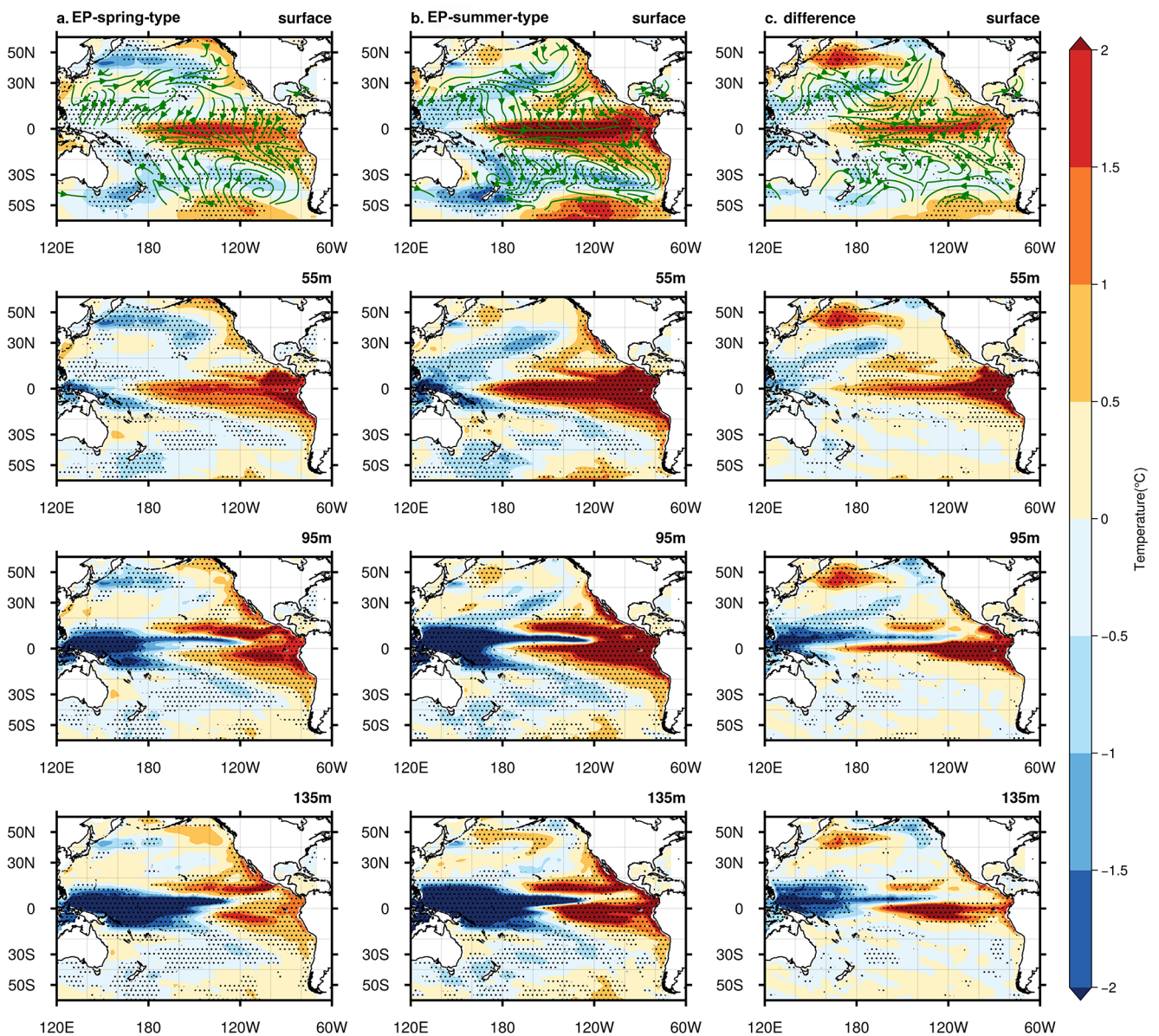


Fig. 12 EP-spring-type (column a) and EP-summer-type (column b) initial error of sea surface temperatures and surface winds that lead to significant spring PB and summer PB in EP-El Niño, and the difference distribution between (EP-summer-type minus EP-spring-type,

column c). Lines 1–4 indicate different ocean depths: 0 m, 55 m, 95 m, 135 m. The initial error in the dotted part of the figure passes the 95% significant t-test

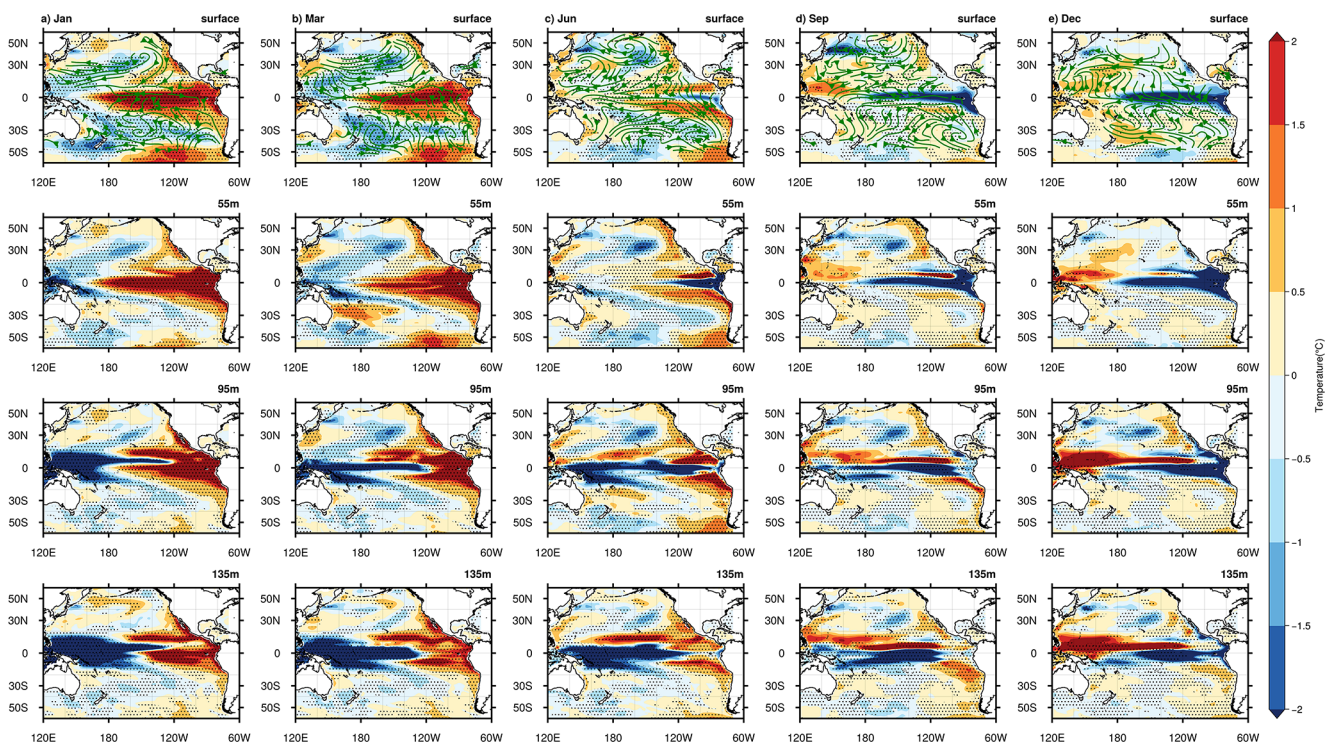


Fig. 13 EP-summer-type sea temperature (unit: °C) and sea surface wind field (unit: m/s) initial error in (a) January, (b) March, (c) June, (d) September, (e) December. Each row represents an ocean depth of 0 m, 55 m, 95 m, and 135 m from top to bottom. The dotted area in the figure passed the 95% significant t-test

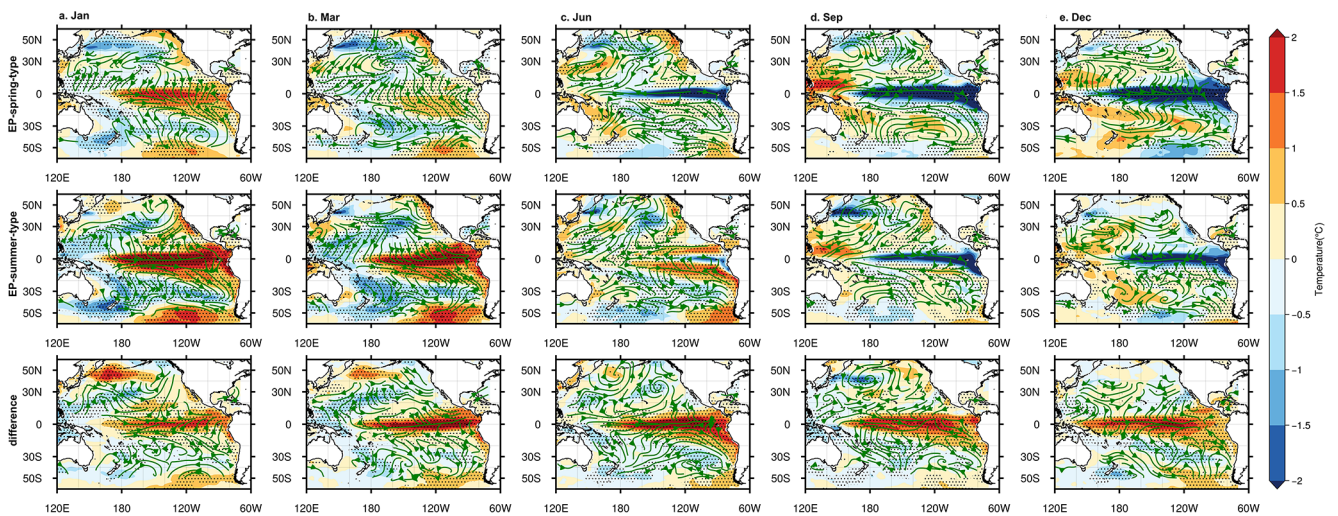


Fig. 14 The difference between EP-summer-type and EP-spring-type SST (unit: °C) and sea surface wind field (in m/s) error evolution in (a) January, (b) March, (c) June, (d) September, and (e) December (EP-summer-type minus EP-spring-type). The dotted areas in the graphs pass the 95% significance t-test

during evolution. The results analyzed above also coincide with many studies that have argued that variabilities from the tropical Pacific as precursor signals for ENSO predictability, especially for EP- El Niño (Bjerknes 1969; Wang et al. 2019a, b; Cai et al. 2020).

In the above study, we investigate whether the initial error in the VM region and tropical Pacific affects the seasonal

variation of the PB for CP- and EP- El Niño. It is found that, for CP-El Niño, based on comparable SST strengths in the tropical Pacific, the VM-like mode error in the North Pacific determines the rate of error evolutions and the season of SST signal transition. On the other hand, for the EP-El Niño, with comparable error amplitudes in the North Pacific, it is the initial SST error in the tropical Pacific background

field that decisively regulates the process. Therefore, it is necessary to consider the influence of the initial error from extratropics and tropical simultaneously when it comes to PB seasonal variation resulting from ENSO diversity.

Why do the initial errors in the CP-El Niño predictions tend to have greater amplitude positive initial error in the North VM region and central-eastern tropical Pacific? Firstly, the VM mode anomaly as the NPO-forced SST seasonal footprint has been mentioned in studies as a possible reason for the onset of CP-El Niño occurrence and a precursor for predicting ENSO diversity (Yu and Kao 2007; Yeh et al. 2015; Wang et al. 2019b; Ding et al. 2022). Meanwhile, Shi et al. (2022; 2023) proposed that the SSTA signal of CP-El Niño transit later than EP-El Niño, with both exhibiting positive VM events, while the evolution is slower during a stronger VM. Therefore, the initial error of CP-El Niño predictions is naturally more strongly correlated with the great amplitude of positive error in the tropical Pacific and strong positive VM-like mode error, which makes the error evolve slower and the error signal transits later. In contrast, EP predictions are more likely to have the opposite characteristics. It explains why the CP-summer-type has a positive error advantage over the EP-spring-type initial error in the tropical Pacific and North Pacific VM regions, allowing for later evolution of the SST error from positive to negative in the eastern Pacific, whereby the PB of CP predictions occurs in summer, PB of EP predictions occurs in spring.

6 Summary and discussion

This study employs a novel predictability data analysis method developed by Hou et al. (2019) to investigate the error growth dynamics associated with summer and spring PB in CP- and EP-El Niño predictions, utilizing monthly pi-control data from the CCSM4 model in CMIP5. By tracking error evolution, our findings indicate that summer PB is predominantly observed in CP-El Niño predictions, whereas spring PB is primarily observed in EP-El Niño predictions.

To take a step further, the two types of initial errors most likely to lead to spring PB for EP-El Niño and summer PB for CP-El Niño are selected and denoted as EP-spring-type and CP-summer-type errors, respectively. The two types of errors are very similar in pattern, presenting SST errors in the North Pacific with a VM-like structure, a dipolar structure of surface-subsurface temperatures in the equatorial Pacific, with positive error in the upper central-eastern Pacific and negative error in the subsurface of the equatorial western Pacific, and SST errors with a SPM-like structure in the extratropical southeast Pacific. Both types of initial errors evolve like an El Niño-like decaying pattern and then rapidly shift to a growth phase similar to a La Niña event.

In addition, it is found that the onset of significant PB occurs during the positive-to-negative transition phase of the SST error in the central-eastern Pacific. By comparing the two types of initial error, the results show that the CP-summer-type initial error exhibits a more significant positive error in the equatorial central-eastern Pacific and a stronger VM-like mode than the EP-spring-type initial error. In the evolution process of the CP-summer-type initial errors, the stronger positive initial error than EP-spring-type in the central-eastern equatorial Pacific costs more time to fully dissipate, resulting in a later appearance of the negative SST error. Additionally, the more pronounced positive error in the VM region for the CP-summer-type initial error hinders the dissipation of the tropical Pacific positive SST errors through the WES mechanism. Both above mechanisms lead to the delayed emergence of the positive-to-negative phase transitions of the SST errors in the tropical Pacific. Therefore, the CP-summer-type prediction experiences a summer PB, rather than a spring PB for the EP-spring-type prediction (see Fig. 15).

Besides, it has been found that seasonal variation of the PB occurrence also appears in the same type of El Niño predictions. Specifically, not all CP(EP)-El Niño predictions interfere with summer (spring) PB. Some CP(EP)-El Niño predictions tend to experience spring (summer) PB. To explore what kind of initial error causes spring PB for CP-El Niño, we analyzed the spatial distribution and evolution of the CP-spring-type error and compared it with the CP-summer-type. The structure and intensity distributions of CP-spring-type are quite similar to CP-summer-type error in the tropics and South Pacific but differ in the VM region of the North Pacific. During the evolution of the CP-spring-type error, the equatorial Pacific SST also undergoes a positive-to-negative phase transition. However, the lack of VM-like positive error in the CP-spring-type error allows the faster dissipation of positive SST errors in the equatorial central-eastern Pacific and earlier transition in spring during the error evolution, thus leading to spring PB for CP-spring-type predictions, instead of summer PB for CP-summer-type predictions. A similar comparison occurs for EP-summer-type and EP-spring-type errors. The two errors do not differ significantly in the extra-equatorial Pacific but bear the most notable difference in the magnitude of the initial positive error in the eastern tropical Pacific. Exhibiting stronger positive error in the eastern tropical Pacific, the EP-summer-type error evolves similar to an El Niño decay and then a La Niña development, but with slower dissipation of the positive error and later shift for the SST error signal, delaying the PB until summer.

Based on our results, it is inferred that the season of the PBs is primarily determined by the SST error transitioning from positive to negative in the central-eastern tropical

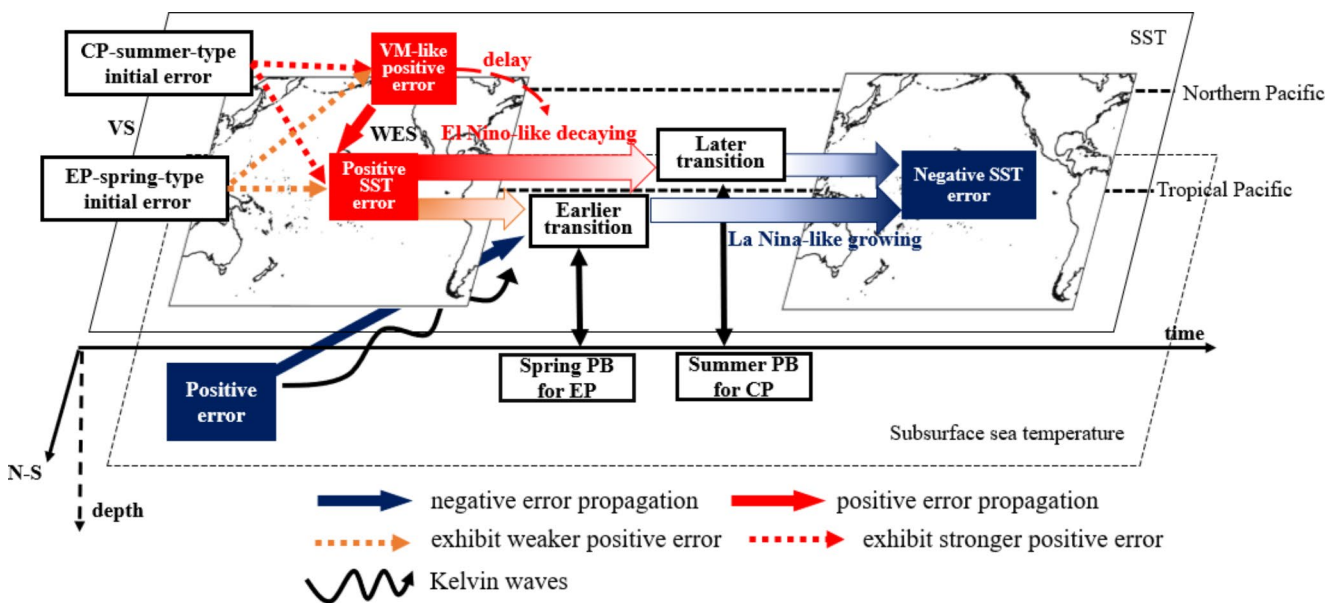


Fig. 15 Diagrams of how different initial errors evolve and propagate, and their impact on the seasons of PBs

Pacific. In addition, the large initial error centers in the northeast Pacific and the tropical Pacific play important roles in determining the occurrence season of PB for two types of El Niño predictions. Precisely, both the VM-like initial error and the initial error in the central-eastern Pacific with dipolar structure determines the transition time, thus leading to distinct PB prevail in different types of El Niño predictions, namely the spring PB for EP-El Niño predictions and the summer PB for CP-El Niño. Besides, when it comes to seasonal variation of PB occurrence in the same type of El Niño predictions, it is found that PB seasonal variations in CP-El Niño predictions are more sensitive to the North Pacific VM error amplitude, whereas EP predictions are more sensitive to the initial error amplitude of the tropical Pacific background. The above implications suggest that when discussing the predictability of ENSO diversity, it is necessary to consider the effects of regions in the whole Pacific comprehensively rather than discussing the different parts separately, which is in line with Shi et al. (2022). These findings also stress the important role of the VM mode on SST in the tropical Pacific, which sheds light on why the CP-El Niño tends to occur PB in summer.

Previous research about PB occurrence concentrated on the annual cycle and the ENSO itself. This study, however, primarily focused on the impact of initial error on the occurrence of PB in El Niño predictions. The initial errors that are most likely to lead to different seasonal PBs for two types of El Niño are identified and compared with each other. Why CP- and EP-El Niño predictions tend to have characteristics like CP-summer-type and EP-spring-type errors was also illustrated. Shi et al. (2023), through analyzing observational and model data, pointed out that based

on the positive VM mode triggering the initial warming in the central tropical Pacific, the rate of SSTA transition in the tropical Pacific determines the ENSO diversity, which is mainly demonstrated by the fact that a slow SSTA transition rate triggers the CP-El Niño, and vice versa for the EP-El Niño. Whereas, Shi et al. (2022) have demonstrated that the positive VM event, which is strongly associated with the formation of CP, contributes to the SSTA persistence and delays the SSTA transition. The previous findings support the conclusion of this study that CP-El Niño prediction exhibits PB to occur in the summertime due to the initial positive SST error dominance in the VM region and tropical Pacific, while EP-El Niño predictions experience a spring PB due to its lack of such a dominance.

In addition, the charging oscillator model of ENSO proposed by Jin (1997a, b) describes the ENSO dynamics as an interaction between the eastern tropical Pacific SST and subsurface heat content (thermocline depth; h). However, our study focuses more on the variables that SST and sea temperature at different depths (θ), the latter also reflects the magnitude of subsurface heat content, thus it can be used to some extent as a substitute for thermocline depth to explore the predictability of ENSO, as has been done in many past studies (Hou et al. 2019; Tao et al. 2020; Qi et al. 2024). Moreover, the classical ENSO dynamical theory does not take into account the effects of extratropical regions, but the scope of our study includes not only the tropics but also extratropical, so it is not as effective as considering depth h in extratropical regions as SST.

The approach to data analysis of ENSO predictability used in this study is clear in principle and allows the analysis of error dynamics without the need to run the numerical

model. Useful conclusions were obtained that can provide a theoretical basis for advancing forecasting skills of El Niño diversity. Besides, several studies have emphasized the role of the Atlantic Ocean in modulating the formation of ENSO diversity (Ham et al. 2013a, b; Dommenges and Yu 2017). Further investigations could be launched to focus on the Atlantic influence on the PB in ENSO predictions.

Acknowledgements The study is supported by the National Natural Science Foundation of China (Grant Nos. 42330111 and 42106004).

Author contributions Can You: Conceptualization, Formal analysis, Investigation, Software, Visualization, Writing – original draft. Meiyi Hou: Conceptualization, Funding acquisition, Methodology, Supervision, Writing – review & editing. Wansuo Duan: Conceptualization, Funding acquisition, Project administration, Writing – review & editing.

Funding This research was jointly supported by the National Natural Science Foundation of China (Grant Nos. 42330111 and 42106004).

Data availability The CCSM4 model output from CMIP5 (Gent et al. 2011) used in this study is available through the websites <https://esgf-node.llnl.gov/search/cmip5/>.

Declarations

Competing interests The authors have no relevant financial or non-financial interests to disclose.

References

- Barnston AG, Tippett MK, L'Heureux ML, Li S, DeWitt DG (2012) Skill of real-time seasonal ENSO model predictions during 2002–11: is our capability increasing? *Bull Am Meteorol Soc* 93(5):631–651. <https://doi.org/10.1175/BAMS-D-11-00111.1>
- Bjerknes J, Atmospheric teleconnections from the equatorial Pacific 1 (1969) *Mon Wea Rev* 97(3):163–172. [https://doi.org/10.1175/1520-0493\(1969\)097%3C0163:ATFTEP%3E2.3.CO;2](https://doi.org/10.1175/1520-0493(1969)097%3C0163:ATFTEP%3E2.3.CO;2)
- Bond NA, Overland JE, Spillane M, Stabeno P. Recent shifts in the state of the North Pacific: recent shifts in the state of the north Pacific. *Geophys Res Lett* 2003;30(23). <https://doi.org/10.1029/2003GL018597>
- Cai W, McPhaden MJ, Grimm AM, Rodrigues RR, Taschetto AS, Garreaud RD, Dewitte B, Poveda G, Ham Y-G, Santoso A, Ng B, Anderson W, Wang G, Geng T, Jo H-S, Marengo JA, Alves LM, Osman M, Li S, Wu L, Karamperidou C, Takahashi K, Vera C (2020) Climate impacts of the El Niño–Southern Oscillation on South America. *Nat Rev Earth Environ* 1(4):215–231. <https://doi.org/10.1038/s43017-020-0040-3>
- Cao Q, Hao Z, Yuan F, Su Z, Berndtsson R, Hao J, Nyima T (2017) Impact of ENSO regimes on developing- and decaying-phase precipitation during rainy season in China. *Hydrol Earth Syst Sci* 21(11):5415–5426. <https://doi.org/10.5194/hess-21-5415-2017>
- Capotondi A (2013) ENSO diversity in the NCAR CCSM4 climate model: ENSO Diversity in the NCAR CCSM4. *J Geophys Res Oceans* 118(10):4755–4770. <https://doi.org/10.1002/jgrc.20335>
- Chou C, Lo M-H (2007) Asymmetric responses of Tropical Precipitation during ENSO. *J Clim* 20(14):3411–3433. <https://doi.org/10.1175/JCLI4197.1>
- Davey MK, Brookshaw A, Ineson S (2014) The probability of the impact of ENSO on precipitation and near-surface temperature. *Clim Risk Manage* 1(C):5–24. <https://doi.org/10.1016/j.crm.2013.12.002>
- Ding R, Tseng Y, Di Lorenzo E, Shi L, Li J, Yu J-Y, Wang C, Sun C, Luo J-J, Ha K, Hu Z-Z, Li F (2022) Multi-year El Niño events tied to the North Pacific Oscillation. *Nat Commun* 13(1):3871. <https://doi.org/10.1038/s41467-022-31516-9>
- Dommenges D, Yu Y (2017) The effects of remote SST forcings on ENSO dynamics, variability and diversity. *Clim Dyn* 49(7–8):2605–2624. <https://doi.org/10.1007/s00382-016-3472-1>
- Duan W, Hu J (2016) The initial errors that induce a significant spring predictability barrier for El Niño events and their implications for target observation: results from an earth system model. *Clim Dyn* 46(11–12):3599–3615. <https://doi.org/10.1007/s00382-015-2789-5>
- Duan W, Wei C (2013) The ‘spring predictability barrier’ for ENSO predictions and its possible mechanism: results from a fully coupled model: spring predictability barrier for ENSO events. *Int J Climatol* 33(5):1280–1292. <https://doi.org/10.1002/joc.3513>
- Feng J, Lian T, Ying J, Li J, Li G (2020) Do CMIP5 models show El Niño Diversity? *J Clim* 33(5):1619–1641. <https://doi.org/10.1175/JCLI-D-18-0854.1>
- Freund MB, Brown JR, Henley BJ, Karoly DJ, Brown JN (2020) Warming patterns affect El Niño Diversity in CMIP5 and CMIP6 models. *J Clim* 33(19):8237–8260. <https://doi.org/10.1175/JCLI-D-19-0890.1>
- Ge Y, Luo D (2023) Impacts of the different types of El Niño and PDO on the winter sub-seasonal north American zonal temperature dipole via the variability of positive PNA events. *Clim Dyn* 60(5–6):1397–1413. <https://doi.org/10.1007/s00382-022-06393-z>
- Gent PR, Danabasoglu G, Donner LJ, Holland MM, Hunke EC, Jayne SR, Lawrence DM, Neale RB, Rasch PJ, Vertenstein M, Worley PH, Yang Z-L, Zhang M (2011) The Community Climate System Model Version 4. *J Clim* 24(19):4973–4991. <https://doi.org/10.1175/2011JCLI4083.1>
- Grimm AM, Tedeschi RG (2009) ENSO and Extreme Rainfall events in South America. *J Clim* 22(7):1589–1609. <https://doi.org/10.1175/2008JCLI2429.1>
- Ham Y-G, Kug J-S (2014) ENSO phase-locking to the boreal winter in CMIP3 and CMIP5 models. *Clim Dyn* 43(1–2):305–318. <https://doi.org/10.1007/s00382-014-2064-1>
- Ham Y, Kug J, Park J (2013a) Two distinct roles of Atlantic SSTs in ENSO variability: North Tropical Atlantic SST and Atlantic Niño. *Geophys Res Lett* 40(15):4012–4017. <https://doi.org/10.1002/grl.50729>
- Ham Y-G, Kug J-S, Park J-Y, Jin F-F (2013b) Sea surface temperature in the north tropical Atlantic as a trigger for El Niño/Southern Oscillation events. *Nat Geosci* 6(2):112–116. <https://doi.org/10.1038/ngeo1686>
- Hou M, Duan W, Zhi X (2019) Season-dependent predictability barrier for two types of El Niño revealed by an approach to data analysis for predictability. *Clim Dyn* 53(9–10):5561–5581. <https://doi.org/10.1007/s00382-019-04888-w>
- Jeong H-I, Lee DY, Ashok K, Ahn J-B, Lee J-Y, Luo J-J, Schemm J-KE, Hendon HH, Braganza K, Ham Y-G (2012) Assessment of the APCC coupled MME suite in predicting the distinctive climate impacts of two flavors of ENSO during boreal winter. *Clim Dyn* 39(1–2):475–493. <https://doi.org/10.1007/s00382-012-1359-3>
- Jin F-F (1997a) An equatorial ocean recharge paradigm for ENSO. Part I: conceptual model. *J Atmos Sci* 54(7):811–829. [https://doi.org/10.1175/1520-0469\(1997\)054%3C0811:AEORPF%3E2.0.CO;2](https://doi.org/10.1175/1520-0469(1997)054%3C0811:AEORPF%3E2.0.CO;2)

- Jin F-F (1997b) An Equatorial Ocean Recharge Paradigm for ENSO. Part II: a stripped-down coupled model. *J Atmos Sci* 54(7):830–847. [https://doi.org/10.1175/1520-0469\(1997\)054%3C0830:AEORPF%3E2.0.CO;2](https://doi.org/10.1175/1520-0469(1997)054%3C0830:AEORPF%3E2.0.CO;2)
- Kao H-Y, Yu J-Y (2009) Contrasting Eastern-Pacific and Central-Pacific types of ENSO. *J Clim* 22(3):615–632. <https://doi.org/10.1175/2008JCLI2309.1>
- Kug J-S, Jin F-F, An S-I (2009) Two types of El Niño events: Cold Tongue El Niño and warm Pool El Niño. *J Clim* 22(6):1499–1515. <https://doi.org/10.1175/2008JCLI2624.1>
- Lee RW-K, Tam C-Y, Sohn S-J, Ahn J-B (2018) Predictability of two types of El Niño and their climate impacts in boreal spring to summer in coupled models. *Clim Dyn* 51(11–12):4555–4571. <https://doi.org/10.1007/s00382-017-4039-5>
- Levine AFZ, Jin F-F (2010) Noise-Induced Instability in the ENSO recharge Oscillator. *J Atmos Sci* 67(2):529–542. <https://doi.org/10.1175/2009JAS3213.1>
- Liu M, Ren H-L, Zhang R, Ineson S, Wang R (2021) ENSO phase-locking behavior in climate models: from CMIP5 to CMIP6. *Environ Res Commun* 3(3):031004. <https://doi.org/10.1088/2515-7620/abf295>
- Masuda S, Matthews JP, Ishikawa Y, Mochizuki T, Tanaka Y, Awaji T (2015) A new Approach to El Niño Prediction beyond the spring season. *Sci Rep* 5:16782. <https://doi.org/10.1038/srep16782>
- McPhaden MJ (2015) Playing hide and seek with El Niño. *Nat Clim Change* 5(9):791–795. <https://doi.org/10.1038/nclimate2775>
- Min Q, Su J, Zhang R (2017) Impact of the South and North Pacific Meridional Modes on the El Niño–Southern Oscillation: observational analysis and comparison. *J Clim* 30(5):1705–1720. <https://doi.org/10.1175/JCLI-D-16-0063.1>
- Mu M, Duan W, Wang B (2007a) Season-dependent dynamics of nonlinear optimal error growth and El Niño–Southern Oscillation predictability in a theoretical model: El Niño predictability dynamics. *J Geophys Res* 112(D10). <https://doi.org/10.1029/2005JD006981>
- Mu M, Xu H, Duan W (2007b) A kind of initial errors related to spring predictability barrier for El Niño events in Zebiak–Cane model. *Geophys Res Lett* 34(3):L03709. <https://doi.org/10.1029/2006GL027412>
- Neelin JD (1991) The slow Sea Surface Temperature Mode and the fast-Wave Limit: Analytic Theory for Tropical Interannual oscillations and experiments in a hybrid coupled Model. *J Atmos Sci* 48(4):584–606. [https://doi.org/10.1175/1520-0469\(1991\)048%3C0584:TSSSTM%3E2.0.CO;2](https://doi.org/10.1175/1520-0469(1991)048%3C0584:TSSSTM%3E2.0.CO;2)
- Qi Q, Duan W, Zheng F, Tang Y (2017) On the spring predictability barrier for strong El Niño events as derived from an intermediate coupled model ensemble prediction system. *Sci China Earth Sci* 60(9):1614–1631. <https://doi.org/10.1007/s11430-017-9087-2>
- Qi Q, Duan W, Liu X, Xu H (2024) Exploring sensitive area in the whole pacific for two types of El Niño predictions and their implication for targeted observations. *Front Earth Sci* 12:1429003. <https://doi.org/10.3389/feart.2024.1429003>
- Rasmusson EM, Wallace JM (1983) Meteorological aspects of the El Niño/Southern Oscillation. *Science* 222(4629):1195–1202. <https://doi.org/10.1126/science.222.4629.1195>
- Ren H, Jin F, Tian B, Scaife AA (2016) Distinct persistence barriers in two types of ENSO. *Geophys Res Lett* 43(20). <https://doi.org/10.1002/2016GL071015>
- Ren H-L, Scaife AA, Dunstone N, Tian B, Liu Y, Ineson S, Lee J-Y, Smith D, Liu C, Thompson V, Vellinga M, MacLachlan C (2019) Seasonal predictability of winter ENSO types in operational dynamical model predictions. *Clim Dyn* 52(7–8):3869–3890. <https://doi.org/10.1007/s00382-018-4366-1>
- Ropelewski CF, Halpert MS (1987) Global and Regional Scale precipitation patterns Associated with the El Niño/Southern Oscillation. *Mon Wea Rev* 115(8):1606–1626. [https://doi.org/10.1175/1520-0493\(1987\)115%3C1606:GARSPP%3E2.0.CO;2](https://doi.org/10.1175/1520-0493(1987)115%3C1606:GARSPP%3E2.0.CO;2)
- Shi L, Ding R, Hu S, Li J, Tseng Y, Li X (2022) Influence of the North Pacific Victoria Mode on the spring persistence barrier of ENSO. *JGR Atmos* 127(9):e2021JD036206. <https://doi.org/10.1029/2021JD036206>
- Shi L, Ding R, Hu S, Mao J, Li J, Tseng Y (2023) Joint effect of the North Pacific Victoria mode and the tropical Pacific on El Niño diversity. *Clim Dyn* 61(1–2):151–168. <https://doi.org/10.1007/s00382-022-06550-4>
- Sohn S-J, Tam C-Y, Jeong H-I (2016) How do the strength and type of ENSO affect SST predictability in coupled models. *Sci Rep* 6(1):33790. <https://doi.org/10.1038/srep33790>
- Tang Y, Zhang R-H, Liu T, Duan W, Yang D, Zheng F, Ren H, Lian T, Gao C, Chen D, Mu M (2018) Progress in ENSO prediction and predictability study. *Natl Sci Rev* 5(6):826–839. <https://doi.org/10.1093/nsr/nwy105>
- Tao L, Duan W, Vannitsem S (2020) Improving forecasts of El Niño diversity: a nonlinear forcing singular vector approach. *Clim Dyn* 55(3–4):739–754. <https://doi.org/10.1007/s00382-020-05292-5>
- Tian B, Duan W (2016) Comparison of the initial errors most likely to cause a spring predictability barrier for two types of El Niño events. *Clim Dyn* 47(3–4):779–792. <https://doi.org/10.1007/s00382-015-2870-0>
- Tseng Y, Huang J, Chen H (2022) Improving the predictability of two types of ENSO by the characteristics of extratropical precursors. *Geophys Res Lett* 49(3). <https://doi.org/10.1029/2021gl097190>
- Vimont DJ, Alexander MA, Newman M (2014) Optimal growth of Central and East Pacific ENSO events. *Geophys Res Lett* 41(11):4027–4034. <https://doi.org/10.1002/2014GL059997>
- Wang C (2018) A review of ENSO theories. *Natl Sci Rev* 5(6):813–825. <https://doi.org/10.1093/nsr/nwy104>
- Wang B, Luo X, Yang Y-M, Sun W, Cane MA, Cai W, Yeh S-W, Liu J (2019a) Historical change of El Niño properties sheds light on future changes of extreme El Niño. *Proc Natl Acad Sci USA* 116(45):22512–22517. <https://doi.org/10.1073/pnas.1911130116>
- Wang X, Guan C, Huang RX, Tan W, Wang L (2019b) The roles of tropical and subtropical wind stress anomalies in the El Niño Modoki onset. *Clim Dyn* 52(11):6585–6597. <https://doi.org/10.1007/s00382-018-4534-3>
- Wang P, Tam C-Y, Lau N-C, Xu K (2021) Future impacts of two types of El Niño on east Asian rainfall based on CMIP5 model projections. *Clim Dyn* 56(3–4):899–916. <https://doi.org/10.1007/s00382-020-05510-0>
- Webster PJ (1995) The annual cycle and the predictability of the tropical coupled ocean-atmosphere system. *Meteorol Atmos Phys* 56(1–2):33–55. <https://doi.org/10.1007/BF01022520>
- Webster PJ, Yang S (1992) Monsoon and ENSO: selectively interactive systems. *QJ Royal Met Soc* 118(507):877–926. <https://doi.org/10.1002/qj.49711850705>
- Xie S-P, Philander SGH (1994) A coupled ocean-atmosphere model of relevance to the ITCZ in the eastern Pacific. *Tellus A: Dynamic Meteorol Oceanogr* 46(4):340. <https://doi.org/10.3402/tellusa.v46i4.15484>
- Yao J, Duan W, Qin X (2021) Which features of the SST forcing error most likely disturb the Simulated Intensity of Tropical Cyclones? *Adv Atmos Sci* 38(4):581–602. <https://doi.org/10.1007/s00376-020-0073-z>
- Yeh S-W, Wang X, Wang C, Dewitte B (2015) On the relationship between the North Pacific Climate variability and the Central Pacific El Niño. *J Clim* 28(2):663–677. <https://doi.org/10.1175/jcli-d-14-00137.1>
- Yu J, Kao H (2007) Decadal changes of ENSO persistence barrier in SST and ocean heat content indices:

- 1958–2001. *J Geophys Res* 112(D13):2006JD007654. <https://doi.org/10.1029/2006JD007654>
- Yu Y, Duan W, Xu H, Mu M (2009) Dynamics of nonlinear error growth and season-dependent predictability of El Niño events in the Zebiak–Cane model. *Quarterly Journal of the Royal Meteorological Society* 135(645):2146–2160. <https://doi.org/10.1016/j.gloplacha.2010.01.021>
- Zhang W, Jin F-F, Li J, Ren H-L (2011) Contrasting impacts of Two-Type El Niño over the Western North Pacific during Boreal Autumn. *J Meteorol Soc Jpn* 89(5):563–569. <https://doi.org/10.2151/jmsj.2011-510>
- Zhang W, Jin F-F, Ren H-L, Li J, Zhao J-X (2012) Differences in Teleconnection over the North Pacific and Rainfall Shift over the USA Associated with two types of El Niño during Boreal Autumn. *J Meteorol Soc Jpn* 90(4):535–552. <https://doi.org/10.2151/jmsj.2012-407>
- Zhang W, Jin F, Stuecker MF, Wittenberg AT, Timmermann A, Ren H, Kug J, Cai W, Cane M (2016) Unraveling El Niño’s impact on the east Asian monsoon and Yangtze River summer flooding. *Geophys Res Lett* 43(21). <https://doi.org/10.1002/2016GL071190>
- Zheng F, Zhu J (2010) Spring predictability barrier of ENSO events from the perspective of an ensemble prediction system. *Glob Planet Change* 72(3):108–117. <https://doi.org/10.1016/j.gloplacha.2010.01.021>
- Zheng Y, Duan W, Tao L, Ma J (2023) Using an ensemble nonlinear forcing singular vector data assimilation approach to address the ENSO forecast uncertainties caused by the spring predictability barrier and El Niño diversity. <https://doi.org/10.1007/s00382-023-06834-3>. *Clim Dyn*

Publisher’s note Springer Nature remains neutral with regard to jurisdictional claims in published maps and institutional affiliations.

Springer Nature or its licensor (e.g. a society or other partner) holds exclusive rights to this article under a publishing agreement with the author(s) or other rightsholder(s); author self-archiving of the accepted manuscript version of this article is solely governed by the terms of such publishing agreement and applicable law.